Chapter 4: Spin state tuning at pseudotetrahedral d^7 ions: examining the structural and magnetic phenomena of 4-coordinate $[BP_3]Co^{II}$-X systems

The text of this chapter is reproduced in part with permission from:

Jenkins, D. M.; Peters, J. C. *J. Am. Chem. Soc.* **2003**, *125*, 11162-11163.

4.1 Introduction

Stereochemical and electronic structure phenomena of the first row transition ions are central issues in coordination chemistry. These properties are strongly coupled, and the experimental determination of one often intimates a great deal about the other. For instance, knowledge of a complex's solid-state crystal structure can reveal its electronic ground state configuration. The four-coordinate first row transition ions Fe(II), Co(II), and Ni(II) are exemplary. Each is high spin when approximately tetrahedral, occupying $S = 2$, $S = 3/2$, and $S = 1$ ground states, respectively. By contrast, when these same ions feature square planar structures, low spin (Co(II) and Ni(II)),[1] or intermediate spin (Fe(II)),[2] ground states are manifest. Knowledge of the interplay between stereochemistry and electronic structure thus lies at the heart of our ability to anticipate magnetic phenomena from key structural parameters. Indeed, the assignment of local stereochemical environments within complex metalloenzyme active sites is often achieved by the interpretation of spectroscopic data.[3,4] Moreover, chemical reactivity can be dramatically affected by subtle spin-state/stereochemical relationships, as in numerous biocatalytic transformations.[5] Inorganic complexes that expose new insights regarding the relationship between stereochemistry and electronic structure are therefore of broad concern.

From the perspective of Ligand Field Theory (LFT), one of the best-studied transition ions is Co^{2+}.[6] The most prominent coordination numbers encountered for this ion are four through six. Six coordinate pseudooctahedral species typically populate high spin configurations, though several low spin systems under the influence of unusually strong ligand fields have been characterized.[7] A host of six-coordinate systems also

exhibit spin crossover phenomena in the solid-state.[8] Sandwich and mixed-sandwich complexes (e.g., $[Cp]_2Co$, $[Cp]CoL_3^+$, [Tp]Co[Cp]; [Tp] = tris(pyrazolyl)borate) constitute a spectroscopically and magnetically rich subset of the octahedral Co(II) family.[9] Five-coordinate Co^{2+} ions exhibit both trigonal bipyramidal and square pyramidal limiting structures. In contrast to the octahedral systems, these five-coordinate ions are most commonly low spin,[10] though again, both spin forms are well-documented, as are systems that exhibit spin crossover in the solid-state.[11,12] Four-coordinate Co(II) systems are nominally either pseudotetrahedral or square planar, though a great many species are known to adopt structures that are highly distorted from these limiting structure types.[13] Nevertheless, prior to recent studies undertaken by our laboratory,[14,15,16] all of the four-coordinate cobalt(II) systems that were known to exhibit low spin ground state configurations were classified as square planar. Ions of approximate tetrahedral geometries, whether nearly perfect T_d symmetry (e.g., $CoCl_4^{2-}$) or species better described as pseudotetrahedral, distorted tetrahedral, or trigonal pyramidal, without exception had been classified as high spin.[17,18,19,20]

Our group has been exploring the nature of highly covalent pseudotetrahedral first row transition ions (L_3M-X) supported by relatively strong field tris(phosphino)borate ligands ($[BP_3]M$-X). The generic abbreviation used to denote these anionic tris(phosphino)borate ligands is $[BP_3]$. $[PhBP_3]$ and $[PhBP^{iPr}_3]$ designate the $[PhB(CH_2PPh_2)_3]^-$ and $[PhB(CH_2P^iPr_2)_3]^-$ anions, respectively (Figure 4.1). These $[BP_3]M$-X systems are striking in their propensity to populate low spin electronic configurations. For example, we have characterized a series of L_3Fe-N_x species that can accommodate low spin ground state configurations for cases where (i) the iron center is

either di-,[21] tri-,[22,23] or tetravalent[24] (i.e., d^6, d^5, or d^4), and (ii) a favorable interaction exists with the N_x-type ligand that is characterized by one sigma and two pi bonds (e.g., $S = 0$, $\{[PhBP_3]Fe^{II}{\equiv}NR\}^-$; S = ½, $[BP_3]Fe^{III}{\equiv}NR$;[22,23] $S = 0$, $[PhBP^{iPr}_3]Fe{\equiv}N$). When the degree of π-bonding is attenuated, as is the situation for the divalent halides $[BP_3]Fe\text{-}X$,[22,25] amides $[PhBP_3]Fe\text{-}NRR'$,[26] alkyls $[PhBP^{iPr}_3]Fe\text{-}R$,[27] and diazenidos $[PhBP^{iPr}_3]Fe\text{-}N{=}NR$, rigorously high spin ($S = 2$) ground states are invariably populated. By contrast, several divalent cobalt ions supported by these $[BP_3]$ platforms populate low spin (S = ½) ground state electronic configurations, even in the absence of a strongly π-bonding X ligand. For example, we have reported that in solution the simple halides $[PhBP_3]CoX$ (X = I, Br, Cl) each exhibit a doublet ground state that is predominantly populated at room temperature. The observed ground spin states of these complexes contrasts not only the numerous tetrahedral and distorted tetrahedral complexes studied previously, but also tripodal borate Co(II) systems that are structurally very similar. These systems include Theopold's[28] and Moro-oka's[29] S = 3/2 [Tp'']CoX ([Tp''] = hydrotris(3-isopropyl-5-methylpyrazoly1)borate species and Riordan's[30] S = 3/2 $[Tt^{tert\text{-}butyl}]CoX$ ($[Tt^{tert\text{-}butyl}] = [PhB(CH_2S^tBu)_3]^-$) derivatives. Moreover, a number of peculiar observations have been reported within the $[BP_3]Co^{II}\text{-}X$ family. For instance, a complex featuring an aryloxide X-type ligand, $[PhBP_3]CoO(2,6\text{-}Me_2\text{-}Ph)$ (**3.4**), exhibits a quartet rather than a doublet ground state. In addition, iodide and chloride complexes of the $[PhBP^{iPr}_3]$ anion ($[PhBP^{iPr}_3]CoI$ and $[PhBP^{iPr}_3]CoCl$) appear to populate rigorously high spin ground states. Each of these observations is somewhat counter-intuitive. The $[PhBP^{iPr}_3]$ anion is more electron-releasing than $[PhBP_3]$, and on the basis of electronic considerations its Co^{2+} complexes should be more likely to populate the low spin

configuration than [$PhBP_3$]Co(II) systems. The same is true of the aryloxide ligand. A more strongly π–donating aryloxide linkage might be expected to more favorably confer a low spin ground state configuration than a halide ligand.

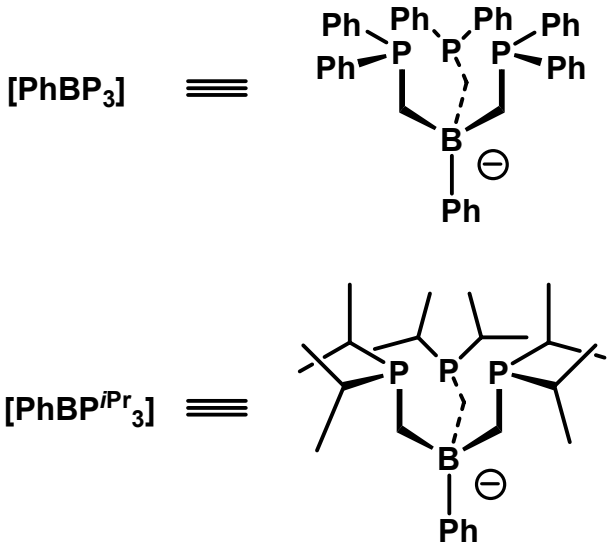

Figure 4.1. Chemical structures of [$PhBP_3$] and [$PhBP^{iPr}_3$].

Perceiving a need to broaden our appreciation of how the interplay between local stereochemistry, the L_3 donor ligand-field strength, and the nature of the X-type ligand work to confer a specific electronic configuration, we set out to systematically characterize a host of pseudotetrahedral d^7 [BP_3]Co-X ions amenable to structure/spin-state correlations. Herein we present the results of this study. Previous studies that have attempted to correlate steric factors with spin-state preferences have emphasized d^6 octahedral systems (e.g., $(L_3)_2$Fe(II)).[31] The systems described in this chapter afford the first opportunity to examine spin-state preferences in *four-coordinate pseudotetrahedral L_3MX structures* by correlating an observed spin-state to the identity of a single X-type ligand, or the identity of an L_3 donor scaffold.

A qualitative sketch of the d-orbital splitting diagrams anticipated for the various limiting stereochemical structures is shown in Figure 4.2. Structures **A** and **B** illustrate the most familiar coordination geometries for four-coordinate Co^{2+} ions. These structure types are square planar (**A**) and tetrahedral (**B**) and give rise to low spin (S = ½) and high spin (S = 3/2) ground state configurations, respectively. An intramolecular distortion that interconverts **A** and **B** is denoted as the "classic case" in Figure 4.2. This phenomenon is well-known for Co(II) ions. Configurational and spin-state equilibria in solution between Co(II) ions of these two limiting structure types is a phenomenon that was lucidly described by Holm and Everett nearly four decades ago.[18,20a] Also, stereochemical tuning of Co(II) complexes using macrocyclic tetradentate ligands can dictate one configuration versus another, and, therefore, different ground spin-states, as exemplified by Lippard and co-workers using tropocoronand ligands.

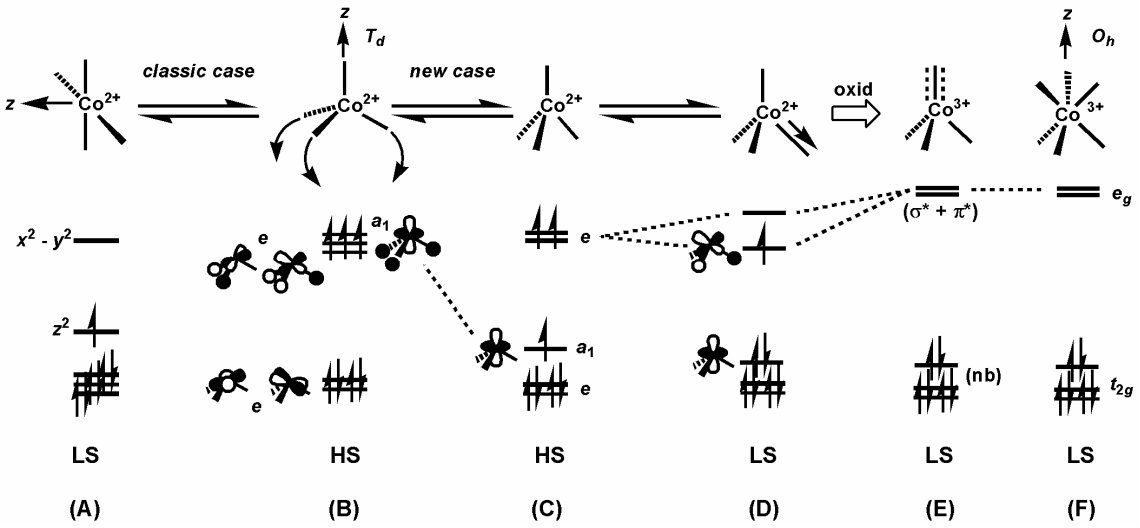

Figure 4.2. Qualitative stereochemical structures and d-orbital splitting diagrams relevant to the four-coordinate structures.

The interconversion between structures **A** and **B** is severe and is likely difficult to access in the crystalline state. A gentler distortion, denoted as the "new case" in Figure 4.2, is one of axial character and produces the pseudotetrahedral structure type **C**. Under three-fold symmetry (C_{3v}) a distortion of this type stabilizes an orbital of a_1 symmetry and provides a d-orbital splitting diagram comprised of $1a_1 + 2e$. This is a familiar orbital arrangement and has been frequently used to describe the electronic structures of sandwich ($[Cp^R]_2M$) and mixed-sandwich ($[Cp^R]ML_3$) complexes.[9,32] For sandwich complexes, the a_1 orbital is most typically placed slightly above a lowest-lying degenerate e-set, though the relative positioning of the lowest three orbitals ($a_1 + e$) has been debated. An important point to underscore is that, to a first approximation, pseudotetrahedral complexes of structure type **C** (i.e., those typically supported by tripodal L_3 donor sets) are electronically best described using a crude "two-over-three" d-orbital splitting diagram akin to that of sandwich complexes like $[Cp]_2Fe$. A tetrahedral splitting diagram is less appropriate. Therefore, while ligands that favor monomeric L_3MX structures are quite often referred to as "tetrahedral enforcers," owing to the pseudotetrahedral stereochemistry they confer, from an electronic structure perspective these ligands might be more appropriately regarded as "octahedral enforcers." The tripodal ligand enforces the requisite axial distortion that gives rise to an approximate two-over-three splitting of the d-orbitals under idealized three-fold symmetry. The ground state electronic structures of three-fold symmetric $[Tp"]Co^{II}$-X complexes are appropriately assigned as $^4A_{2g}$,[28,29,33] but, as discussed further below, these ground states bear a closer electronic relationship to high spin octahedral complexes such as $[Tp]_2Co$[34] than to high spin tetrahedral complexes such as $[Cs]_2[CoCl_4]$.[35] These general ideas help

to account for the relative ease with which complexes of the high spin structure type **C** can crossover to a related but low spin structure type **D** given appropriate choice of the donor ligand set.

4.2 Results and discussion

4.2.1 Synthesis and routine solution characterization of $[BP_3]Co^{II}$-X complexes

To more thoroughly examine structure/spin-state relationships within the $[BP_3]Co^{II}X$ system we prepared a series of $[BP_3]Co^{II}$-X complexes that feature O-atom and S-atom X-type linkages. Table 4.1 lists each of the $[BP_3]Co$ complexes featured in the present study, along with their numerical designations, color, and electrochemical characterization data. The magnetic characterization data are incorporated in Table 4.2. A fair number of alkoxide, aryloxide, thiolate, and arylthiolate derivatives of cobalt have been described previously, and several L_3MX systems that are structurally relevant to the present cobalt derivatives warrant specific mention. For instance, tris(pyrazolyl)borate ([Tp]) derivatives of cobalt[28,29,33] that feature X-type linkages related to the present systems have been reported. There are also several neutral tris(phosphine) Co(I) complexes, for example $(PPh_3)_3CoOPh$,[36,37] though we are unaware of any four-coordinate $P_3Co^{II}X$ species other than those supported by $[BP_3]$ ligands. A tripodal amine donor ligand system that supports complexes with a single aryloxide ligand on cobalt has also been described.[38]

The choice of $[BP_3]Co^{II}$-X complexes that feature O-atom and S-atom X-type linkages was due to the relative ease with which steric and electronic parameters could be tuned in a systematic fashion, and to the ease with which their Co(II) complexes could be generated and purified. Other X-type linkages were considered, for example alkyls and

amides, but these types of complexes have proven to be synthetically problematic within the [BP_3]Co-X family. Attempts to prepare them has led to side reactions indicative of undesirable redox chemistry rather than clean metallation.

Table 4.1. Summary of color and electrochemical data.

Complex Name and Number	Color	Co^{II}/Co^{III}, Co^{I}/Co^{II} (mV)
[$PhBP_3$]CoI, **3.1**	Green	10, -920
[$PhBP_3$]CoOSiPh_3, **4.1**	Purple	-360, -1290
[$PhBP_3$]CoO(4-^{t}Bu-Ph), **4.2**	Red-brown	-390, -1330
[$PhBP_3$]CoO(C_6F_5), **4.3**	Olive green	NA, NA
[$PhBP_3$]CoSPh, **4.4**	Red	-160, -1120
[$PhBP_3$]CoS(2,6-Me_2-Ph), **4.5**	Red	-170, -1100
[$PhBP_3$]CoS(2,4,6-$^{i}Pr_3$-Ph), **4.6**	Red-brown	-80, -1190
[$PhBP_3$]CoS(2,4,6-$^{t}Bu_3$-Ph), **4.7**	Red	-60, -1080
[$PhBP_3$]CoSSiPh_3, **4.8**	Green	-210 (irreversible), -1010
[$PhBP_3$]CoOSi(4-NMe_2-Ph)$_3$, **4.9**	Red	-360, -1300
[$PhBP_3$]CoOSi(4-CF_3-Ph)$_3$, **4.10**	Blue	-60 (irreversible), -1080
[$PhBP_3$]CoOCPh_3, **4.11**	Blue-green	-300, -1310
[$PhBP^{iPr}_3$]CoI, **4.12**	Green	60, -1250
[$PhBP^{iPr}_3$]CoOSiPh_3, **4.13**	Purple	100 (irreversible), -1690
[$PhBP^{iPr}_3$]CoSSiPh_3, **4.14**	Green	-140 (irreversible), -1330
{[$PhBP_3$]CoOSiPh_3} {B(3,5-(CF_3)$_2$-Ph)$_4$}, {**4.15**} {B(3,5-(CF_3)$_2$-Ph)$_4$}	Green	Oxidation product of **4.1**

Table 4.2. Summary of magnetic data.

Complex Number	Evans Method (μ_{eff} in BM, C_6D_6, 298 K)	SQUID $\chi_m T$ (cm^3 K mol^{-1}) at 20 K, 300 K
3.1	2.8	0.82, 1.01
4.1	3.4	0.47, 1.45
4.2	3.4	0.90, 1.90
4.3	3.8	1.32, 2.13 (at 240 K)
4.4	2.4	0.40, 0.49
4.5	2.3	0.50, 0.51
4.6	2.8	0.46, 0.63
4.7	3.9	2.05, 2.21
4.8	2.5	0.47, 0.44
4.9	3.5	0.46, 1.56
4.10	3.9	1.22, 1.95
4.11	3.8	2.08, 2.28
4.12	4.1	1.83, 1.90
4.13	4.3	2.19, 2.36
4.14	4.0	0.47, 1.23
{**4.15**} $\{B(3,5\text{-}(CF_3)_2\text{-}Ph)_4\}$	Diamagnetic	Diamagnetic

The family of complexes shown in Table 4.1 is conveniently accessible via the use of the soft thallium reagents TlEAr and $TlEZAr_3$ (E = O or S, Z = Si or C, Eq. 4.1). The typical method for preparation of these thallium reagents involves a metathesis reaction between commercially available thallium ethoxide and the desired phenol, arylthiol, silanol, or silylthiol.[39] The types of alcohols and thiols amenable to this method of preparation are restricted to those that have pK_a values lower than that of the ethanol byproduct (pK_a = 15.9). The addition of one equivalent of the desired thallium reagent as a THF solution to a THF solution of $[BP_3]CoX$ (X = I or Cl) affords the substituted product in high crude yield with TlX as an easily separable byproduct. Filtration of the crude reaction mixture followed by crystallization, typically by vapor diffusion of petroleum ether in benzene, provides each of the desired complexes in crystalline form in modest to high yields.

Despite the paramagnetic nature of these Co(II) derivatives, ^{1}H NMR spectroscopy aids in their characterization. While the signature proton resonances are listed for each isolated complex in the Experimental Section, we examined the paramagnetically shifted ^{1}H NMR spectra of the iodides $[PhBP_3]CoI$ (**3.1**) and $[PhBP^{iPr}_3]CoI$ (**4.12**) in some detail, as a representative sample of this family of complexes. Both complexes exhibit solution spectra (see Figure 4.3) consistent with approximate C_3 symmetry at room temperature, as only a single set of resonances arises from the phosphine donor arms. T_1 relaxation times can be used as a guide to determine the relative distances of ligand-based protons from a coordinated metal center containing unpaired spin.[40] By measuring a T_1 relaxation time for each proton resonance shown in

Figure 4.3 (top and bottom), and correlating these relaxation times with the integrated number of protons corresponding to each resonance, we are able to assign the spectrum of **3.1** with a high degree of confidence. The spectrum of **4.12** suffers from some ambiguity due to certain resonances having similar T_1 relaxation times and integration values. Notably, the chemical shift range of the resonances observed for **4.12** is much broader than that of **3.1**, likely due to their different respective spin states (vide infra).

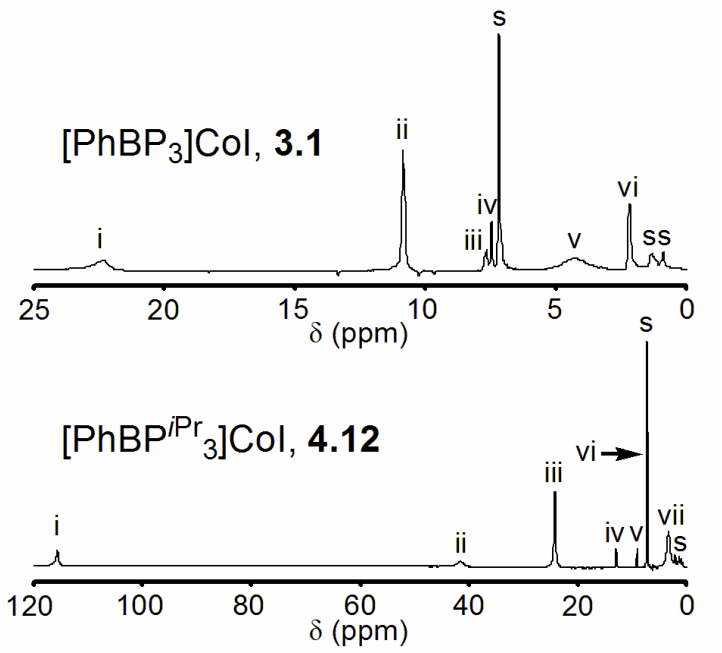

Figure 4.3. ^{1}H NMR spectra of **3.1** and **4.12** in C_6D_6. Assignments are based on the correlation between single scan integration values and T_1 relaxation times for each resonance. For **3.1**: (i) $PhB(CH_2PPh_2)_3$, (ii) *meta* $P(C_6H_5)_2$, (iii) *ortho* $B(C_6H_5)$, (iv) *meta* and *para* $B(C_6H_5)$, (v) *ortho* $P(C_6H_5)_2$, (vi) *para* $P(C_6H_5)_2$. For **4.12**: (i and ii) $PhB(CH_2P^iPr_2)_3$ and $P(CH(CH_3)_2)_2$, (iii and vii) $P(CH(CH_3)_2)_2$, (iv) *ortho* $B(C_6H_5)$, (v) *para* $B(C_6H_5)$, (vi) *meta* $B(C_6H_5)$.

4.2.2 Electrochemical data

The electrochemical response of each complex featured in this study was examined by cyclic voltammetry in THF solution using either $[^nBu_4N][PF_6]$ or $[^nBu_4N][ClO_4]$ as the supporting electrolyte, a glassy carbon working electrode, a platinum wire counter electrode, and a $Ag/AgNO_3$ reference electrode. The potentials of well-defined redox processes were recorded versus an external ferrocene standard and are listed in Table 4.1.

The electrochemical data are generally unremarkable and hence only a few comparative comments are warranted. For those $[PhBP_3]Co(II)$ complexes featuring a Co-OR linkage, specifically complexes **4.1**, **4.2**, **4.3**, **4.9**, **4.10**, and **4.11**, fully reversible Co(II/III) and Co(I/II) redox processes are observed. Relatively little shift in the potential of either redox event is observed within this family, with the exception of the *p*-CF_3-substituted silyloxide species $[PhBP_3]CoOSi(4\text{-}CF_3\text{-}Ph)_3$, **4.10**. For this complex the Co(I/II) redox event is anodically shifted by ca. 300 mV, and the Co(II/III) redox event is irreversible. These differences are likely due to the electron-withdrawing CF_3 substituent, which destabilizes the higher-valent Co(III) state but renders the lower-valent Co(I) state more accessible.

The $[PhBP_3]Co(II)$ arylthiolate complexes **4.4**-**4.8** also exhibit well-behaved Co(II/III) and Co(I/II) redox events. These thiolate species are, as might be expected, easier to reduce and more difficult to oxidize than their aryloxide relatives. Again, only a small degree of variance is observed for the potentials amongst the arylthiolate family of complexes. Two subtle differences worth noting are (i) complexes $[PhBP_3]CoS(2,4,6\text{-}^iPr_3\text{-}Ph)$, **4.6**, and $[PhBP_3]CoS(2,4,6\text{-}^tBu\text{-}Ph)$, **4.7**, are approximately

100 mV more difficult to oxidize than [PhBP$_3$]CoSPh, **4.4**, and [PhBP$_3$]CoS(2,6-Me$_2$-Ph), **4.5**, presumably reflecting the difference in electron-releasing character between the arylthiolate substituents; and (ii) it is ca. 100 mV more difficult to reduce **4.6** than **4.7**, an observation that is difficult to rationalize in simple terms. The triphenylsilylthiolato derivative [PhBP$_3$]CoSSiPh$_3$ (**4.8**) is the most easily reduced species (-1010 mV), but displays an irreversible oxidation event around -210 mV. The reduction potential recorded for complex **4.8** can be compared with that of its [PhBP$^{i\text{Pr}}_3$]-supported congener [PhBP$^{i\text{Pr}}_3$]CoSSiPh$_3$ (**4.14**). The latter complex **4.14** is ca. 300 mV more difficult to reduce (-1330 mV) due to its more electron-releasing P$_3$ donor scaffold, but still displays an irreversible Co(II/III) process. Comparison of the redox processes observed between [PhBP$_3$]CoOSiPh$_3$, **4.1**, and [PhBP$^{i\text{Pr}}_3$]CoOSiPh$_3$, **4.13**, reveals another curiosity of note. While **4.13** is appreciably more difficult to reduce (by ca. 400 mV), as should be expected, its oxidation to Co(III) is electrochemically irreversible. By contrast, {[PhBP$_3$]Co$^{\text{III}}$OSiPh$_3$}$^+$ is electrochemically accessible and stable (vide infra). This is difficult to rationalize, except to suggest that a putative {[PhBP$^{i\text{Pr}}_3$]Co$^{\text{III}}$OSiPh$_3$}$^+$ species may be more prone to loss of the triphenylsilyl substituent in the presence of a fluorinated counter-anion from the electrolyte.

Finally, it is interesting to compare the electrochemical data recorded for these cobalt systems with that of a related series of recently reported [BP$_3$]Ni-X systems.[41] For example, a reversible Ni(I/II) reduction event is observed for the complex [PhBP$_3$]NiOSiPh$_3$ at -1.47 V, which is ca. 180 mV more negative than the Co(I/II) event of **4.1**. More striking is how difficult it is to oxidize the nickel systems to the Ni(III) state. For the complex [PhBP$_3$]NiOSiPh$_3$, the first oxidative process is encountered at a

potential that is ca. 700 mV more positive than for its cobalt analogue **4.1**. This large difference appears to reflect the relative instability of a d^7 versus a d^6 electronic configuration within the $[BP_3]$Ni-X and $[BP_3]$Co-X platforms, respectively.

4.2.3 Chemical oxidation of $[PhBP_3]CoOSiPh_3$ to produce $\{[PhBP_3]CoOSiPh_3\}\{BAr_4\}$

Reversible oxidation waves for these $[BP_3]Co^{II}$-X derivatives suggest that their chemical oxidation might afford the corresponding trivalent $\{[BP_3]Co^{III}\text{-}X\}^+$ products, which would comprise a structurally unusual class of pseudotetrahedral Co(III) complexes (type **E** in Figure 4.2). We have prepared and thoroughly characterized one such example pertinent to the present study: $\{[PhBP_3]CoOSiPh_3\}\{BAr_4\}$, $\{\mathbf{4.15}\}\{BAr_4\}$ (Ar = C_6H_5, 3,5-$(CF_3)_2$-C_6H_3). The addition of THF to a solid mixture of **4.1** and $\{[Cp]_2Fe\}\{BAr_4\}$ effects a rapid oxidation process to generate the diamagnetic, green product $\{\mathbf{4.15}\}\{BAr_4\}$ (Eq. 4.2). Cationic $\{\mathbf{4.15}\}\{BAr_4\}$ exhibits a sharp singlet in its ^{31}P NMR spectrum at 64.6 ppm and also a sharp singlet in the ^{19}F NMR spectrum at -58.5 for the tetra(3,5-bis(trifluoromethyl)phenyl)borate salt derivative. The combined ^1H and ^{31}P NMR spectra obtained for this system reveal that it is threefold symmetric in solution on the NMR time scale. The diamagnetic ground state of $\{\mathbf{4.15}\}^+$ suggests that its electronic configuration is likely related to the diamagnetic imide $[PhBP_3]Co{\equiv}N$-*p*-tolyl, which is an $S = 0$ Co(III) species featuring a bona fide Co-N triple bond linkage.[42] However, whereas $\{\mathbf{4.15}\}^+$ can be reduced at a potential of ca. -360 mV, the imide species $[PhBP_3]Co{\equiv}N$-*p*-tolyl is stable to reduction at potentials as low as ca. – 3.0 V, reflecting both the difference in charge and the weaker strength of the π-bonding in $\{\mathbf{4.15}\}^+$.

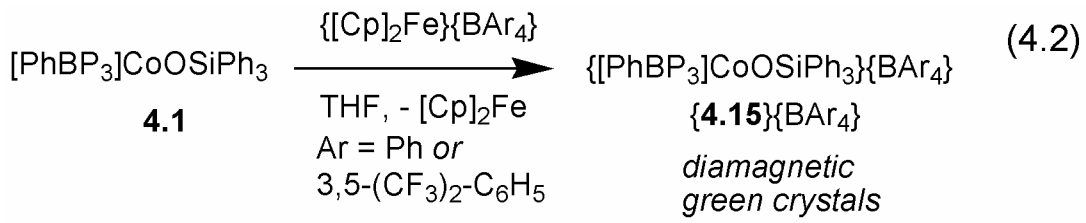

4.2.4 Structural characterization and stereochemical classification of $[BP_3]Co^{II}$-X derivatives

Solid-state crystal structures have been determined for many of the cobalt complexes listed in Table 4.1. These results are summarized by their core structure representations, collected in Figure 4.4 and Figure 4.5, and by a list of salient bond distances and angles, collected in Table 4.3. In each structure, the tris(phosphino)borate is κ^3-bound to a monomeric cobalt center. The pseudotetrahedral structures can be broadly divided into two separate classes based on the average length of the Co-P bonds. As will be corroborated by the SQUID and EPR data discussed below, complexes featuring average Co-P bond distances between 2.15 Å and 2.25 Å (e.g., **4.5** and **4.9**) are characteristic of low spin ground states (type **D** in Figure 4.2), whereas complexes with average Co-P bond distances between 2.30 Å and 2.35 Å (e.g., **4.7** and **4.11**) are characteristic of high spin ground states (type **C** is Figure 4.2).

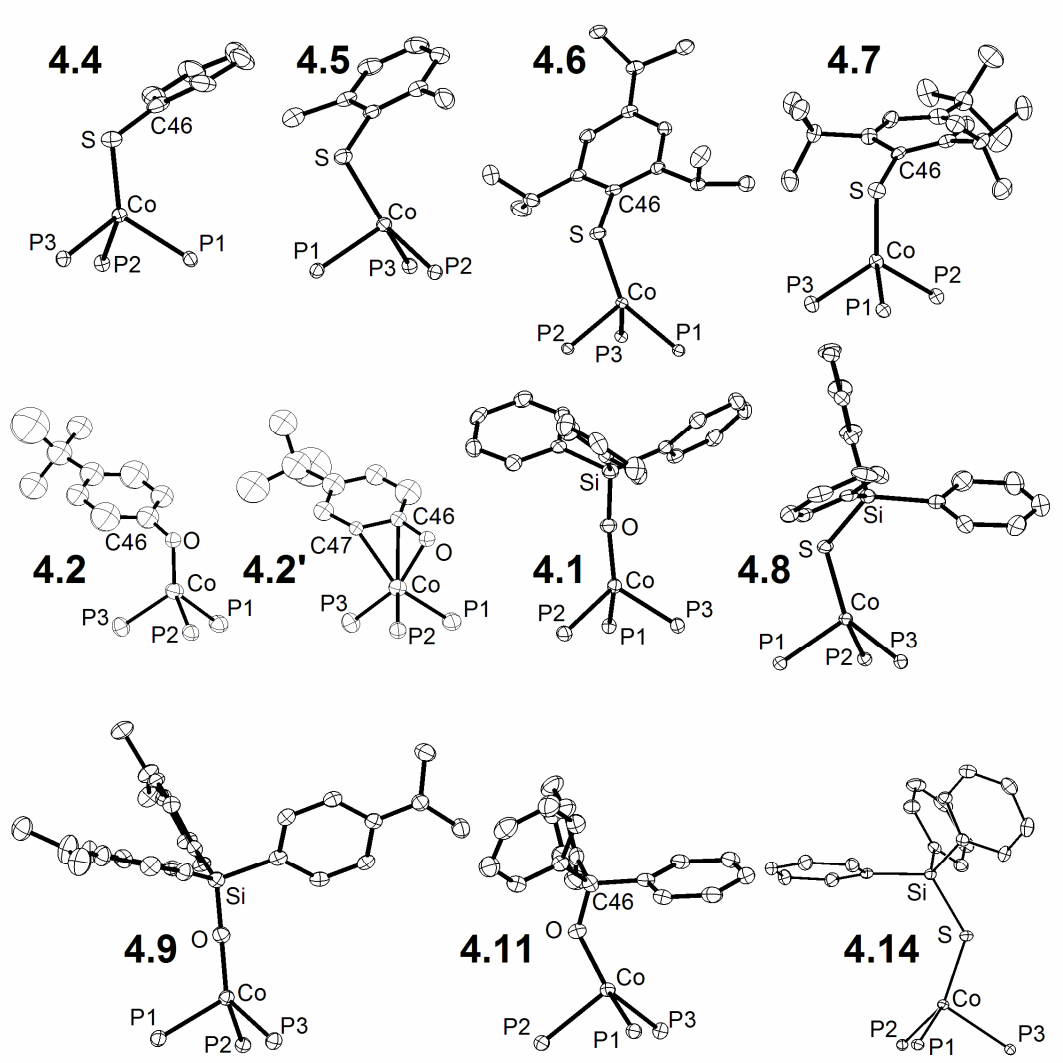

Figure 4.4. Displacement ellipsoid representations (50%) of the core structures of [PhBP$_3$]CoSPh (**4.4**); [PhBP$_3$]CoS(2,6-Me$_2$-Ph) (**4.5**); [PhBP$_3$]CoS(2,4,6-^{i}Pr$_3$-Ph) (**4.6**); [PhBP$_3$]CoS(2,4,6-^{t}Bu$_3$-Ph) (**4.7**); [PhBP$_3$]CoO(4-^{t}Bu-Ph) (**4.2**); [PhBP$_3$]CoOSiPh$_3$ (**4.1**); [PhBP$_3$]CoSSiPh$_3$ (**4.8**); [PhBP$_3$]CoOSi(4-NMe$_2$-Ph)$_3$ (**4.9**); [PhBP$_3$]CoOCPh$_3$ (**4.11**); and [PhBP$^{i\text{Pr}}_3$]CoSSiPh$_3$ (**4.14**). The **4.2** and **4.2**' structures show the disorder in the –O(4-^{t}Bu-Ph) ligand, which is bound either η^1 (left) or η^3 (right) to the cobalt center. See Table 4.3 for bond lengths and angles.

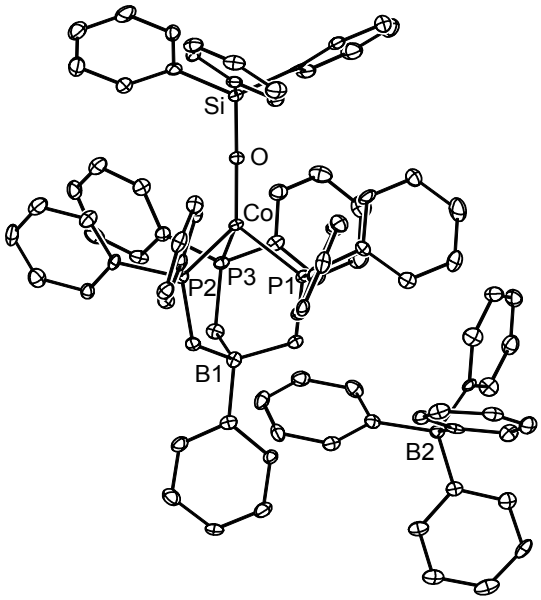

Figure 4.5. Displacement ellipsoid representations (50%) of {[$PhBP_3$]$CoOSiPh_3$}{BPh_4}, {**4.15**}{BPh_4}. Hydrogen atoms and solvent molecules have been omitted for clarity. See Table 4.3 for bond lengths and angles.

The basic stereochemical structures observed in the solid-state can be further classified, at least qualitatively, as having one of two general structure types that we will refer to throughout as either **umbrella** distorted or **off-axis** distorted (Figure 4.6). In an umbrella distorted structure, the X-type ligand is regarded as axial and trisects the three Co-P linkages, coincident with the B-Co vector. Distortions of an umbrella type are common for four-coordinate complexes supported by tripodal ligands, and it may be said that such ligands in fact enforce the umbrella distortion.[28,30] In an off-axis distorted structure, the X-type ligand cants away from the imaginary vector running through the B and Co atoms to such an appreciable extent that it is better regarded as an equatorial

ligand rather than an axial ligand. Four-coordinate complexes that exhibit an off-axis distortion are less frequently encountered and appear to arise from the population of a low spin ground state, as discussed in greater detail below.

Table 4.3. X-ray diffraction table showing key bond lengths (Å) and angles (deg) for **4.1**, **4.2**, **4.4**, **4.5**, **4.6**, **4.7**, **4.8**, **4.9**, **4.11**, **4.14**, and {**4.15**}{BPh_4}.

Complex Name and Number	Co-E[a]	E-Z[b]	Co-P1	Co-P2	Co-P3
[$PhBP_3$]$CoOSiPh_3$, **4.1**	1.799(2)	1.612(2)	2.156(1)	2.284(1)	2.169(1)
[$PhBP_3$]CoO(4-^{t}Bu-Ph), **4.2**[c]	1.832(7)	1.327(8)	2.247(1)	2.230(1)	2.227(1)
[$PhBP_3$]CoO(4-^{t}Bu-Ph), **4.2'**[c]	1.885(4)	1.330(6)	2.247(1)	2.230(1)	2.227(1)
[$PhBP_3$]CoSPh, **4.4**[d]	2.153(1)	1.742(4)	2.175(1)	2.178(1)	2.249(1)
[$PhBP_3$]CoS(2,6-Me_2-Ph), **4.5**	2.167(1)	1.781(2)	2.251(1)	2.199(1)	2.208(1)
[$PhBP_3$]CoS(2,4,6-$^i Pr_3$-Ph), **4.6**[d]	2.155(1)	1.802(2)	2.201(1)	2.280(1)	2.205(1)
[$PhBP_3$]CoS(2,4,6-$^t Bu_3$-Ph), **4.7**	2.207(1)	1.784(5)	2.354(1)	2.351(1)	2.387(1)
[$PhBP_3$]$CoSSiPh_3$, **4.8**	2.190(1)	2.120(1)	2.206(1)	2.167(1)	2.243(1)
[$PhBP_3$]CoOSi(4-NMe_2-Ph)$_3$, **4.9**	1.809(1)	1.618(2)	2.265(1)	2.144(1)	2.194(1)
[$PhBP_3$]$CoOCPh_3$, **4.11**[d]	1.839(1)	1.398(2)	2.349(1)	2.361(1)	2.387(1)
[$PhBP^{iPr}_3$]$CoSSiPh_3$, **4.14**	2.178(1)	2.113(1)	2.179(1)	2.179(1)	2.357(1)
{[$PhBP_3$]$CoOSiPh_3$}{BPh_4}, {**4.15**}{BPh_4}	1.766(3)	1.652(3)	2.187(1)	2.182(1)	2.184(1)

Table 4.3 (cont.)

Complex Number	Co-E-X	P1-Co-P2	P1-Co-P3	P2-Co-P3	P1-Co-E	P2-Co-E	P3-Co-E
4.1	172.5(1)	91.38(3)	85.88(3)	94.60(3)	129.45(7)	119.42(7)	125.82(7)
4.2	110.3(4)	91.48(4)	90.96(4)	96.35(4)	133.4(3)	106.9(2)	127.5(3)
4.2'	88.4(3)	91.48(4)	90.96(4)	96.35(4)	97.6(2)	110.8(1)	151.2(1)
4.4	104.3(1)	89.44(4)	97.52(4)	90.70(4)	121.14(4)	143.46(4)	103.24(4)
4.5	114.6(1)	89.44(2)	100.23(2)	86.73(2)	96.48(2)	147.37(2)	123.30(2)
4.6	123.2(1)	89.26(2)	88.14(2)	98.04(2)	143.37(2)	107.92(2)	119.75(2)
4.7	111.3(2)	96.11(5)	92.81(5)	96.30(5)	109.46(5)	125.24(5)	128.37(6)
4.8	128.0(1)	87.79(3)	99.63(3)	87.65(3)	108.15(3)	139.91(3)	123.62(3)
4.9	165.7(1)	90.43(2)	94.56(2)	86.47(2)	117.36(5)	127.61(5)	129.77(5)
4.11	138.0(1)	92.56(2)	95.67(2)	92.40(2)	126.83(5)	102.99(5)	133.18(5)
4.14	131.5(1)	90.30(2)	92.75(2)	93.27(2)	136.69(2)	126.30(2)	105.64(2)
{**4.15**}{BPh_4}	178.6(2)	90.67(5)	90.18(5)	90.50(5)	125.6(1)	124.4(1)	124.8(1)

Table 4.3 footnotes. a–E represents the fourth, non-phosphine atom directly bound to the Co center, either O or S; **b**–Z represents the non-cobalt atom bound to E, which is either C or Si; **c**–**4.2** shows the bond distances and angles for the η^1 conformation. **4.2'** shows the bond angles and distances for the η^3 conformation; **d**–There are two crystallographically independent molecules in the unit cell.

Rigorously distinguishing between structures that arise from these two limiting distortions is not readily apparent by inspection. An elegant method known as the *continuous symmetry measure*[13,43] proves very useful in this regard because it allows one to quantitatively discuss how close a given molecular geometry is to an idealized structure type. For example Alvarez and co-workers have used this approach to quantitatively compare true geometric structures to those of idealized tetrahedra or square planes. Under a continuous symmetry measurement, the distance (i.e., deviation) of a given molecule from an idealized polyhedron of a symmetry point group defined as *G* is numerically defined as *S(G)*. A perfect tetrahedron therefore has an $S(T_d) = 0$, and a perfect square plane has an $S(D_{4h}) = 0$. Construction of a 2-D plot of *S(G)* values can then be used to show that a perfect tetrahedron has an $S(D_{4h}) = 33.3$, and a perfect square plane has an $S(T_d) = 33.3$. As should be obvious, a trigonal pyramidal structure is geometrically much closer to a tetrahedron than to a square plane. This is reflected by its respective *S(G)* values; it features a relatively small $S(T_d)$ by comparison to a large $S(D_{4h})$ value ($S(T_d) = 3.57$; $S(D_{4h}) = 34.87$).

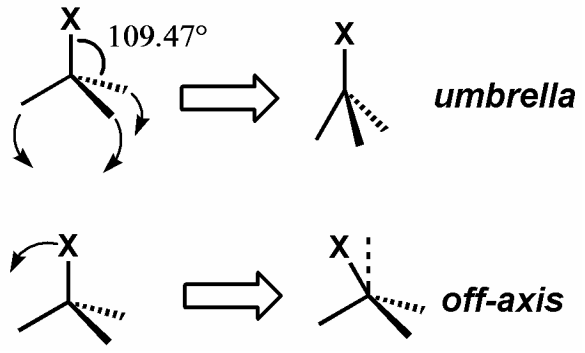

Figure 4.6. Limiting distortions relevant to the pseudotetrahedral structure types.

Plotting the data for the X-ray structures shown in Figures 4.4 and 4.5 on a 2-D continuous symmetry map allows us to see the deviations. Comparing the species on a S(T_d) versus S(D_{4h}) map shows that the complexes we have prepared are all reasonably close to an ideal tetrahedron (Figure 4.7). Complexes on the upper left portion of the graph exhibit a typical umbrella distortion and are high spin (vide infra). This class includes complexes [PhBP$_3$]CoS(2,4,6-^{t}Bu$_3$-Ph) (**4.7**), [PhBP$_3$]CoOCPh$_3$ (**4.11**), and [PhBP$^{i\text{Pr}}_3$]CoI (**4.12**). The ambient temperature solid-state structure of [PhBP$_3$]CoOSiPh$_3$ (**4.1**) is also in this class. The upper right box features low spin umbrella complexes including the siloxides: **4.1** (at 98 K), [PhBP$_3$]CoOSi(4-NMe$_2$-Ph)$_3$ (**4.9**), and {[PhBP$_3$]CoOSiPh$_3$}{BPh$_4$} ({**4.15**}{BPh$_4$}) and the iodide complex we previously reported, [PhBP$_3$]CoI (**3.1**). The complexes we denote as off-axis structure types are somewhat distinct from the [PhBP$_3$]Co^{II}-X complexes we have described in previous studies (lower right box in Figure 4.7).[14,15] These off-axis complexes all incorporate a thiolate as the fourth ligand. Furthermore, all of the off-axis species (**4.4**, **4.5**, **4.6**, **4.8**, and **4.14**) are low spin at 98 K. Not surprisingly, these five complexes feature one elongated Co-P bond in an axial position and two shorter Co-P bonds in the equatorial positions.

Given that all of these P$_3$Co^{II}X species show only a small distortion from an ideal tetrahedron, it is worth examining whether some of the species are better described as trigonal pyramidal. A continuous symmetry plot mapping the deviations from an ideal trigonal pyramid and a tetrahedron is shown in Figure 4.8. Almost all of the complexes fall within the middle portion of the graph, implying roughly equal distortions from both idealized geometries. Complexes **4.1**, **4.9**, **4.12**, and {**4.15**} have less distortion from a

tetrahedron than complex **4.5**, which, while distorted from both idealized geometries, is slightly closer to a trigonal pyramid. It is admittedly difficult to tease out a definitive difference between these two ideal geometries for the structures described. The dotted line shown in Figure 4.8 qualitatively draws the same distinction illustrated by the previous graph (Figure 4.7). The complexes on the left side feature typical umbrella distortions, and the complexes on the right feature off-axis distortions. The single discrepancy between this plot and the plot in Figure 4.7 is that this symmetry map suggests that complex **3.1** belongs to the off-axis class instead of the umbrella class. None of the complexes we have prepared is truly close to a trigonal pyramidal geometry since the equatorial L-Co-L angles are inequivalent. Known examples of trigonal pyramidal Co(II) species have been assigned as high spin and often feature a tetradentate ligand with three equivalent tripodal arms and one axial donor ligand giving equivalent L-Co-L angles near 120°.[17]

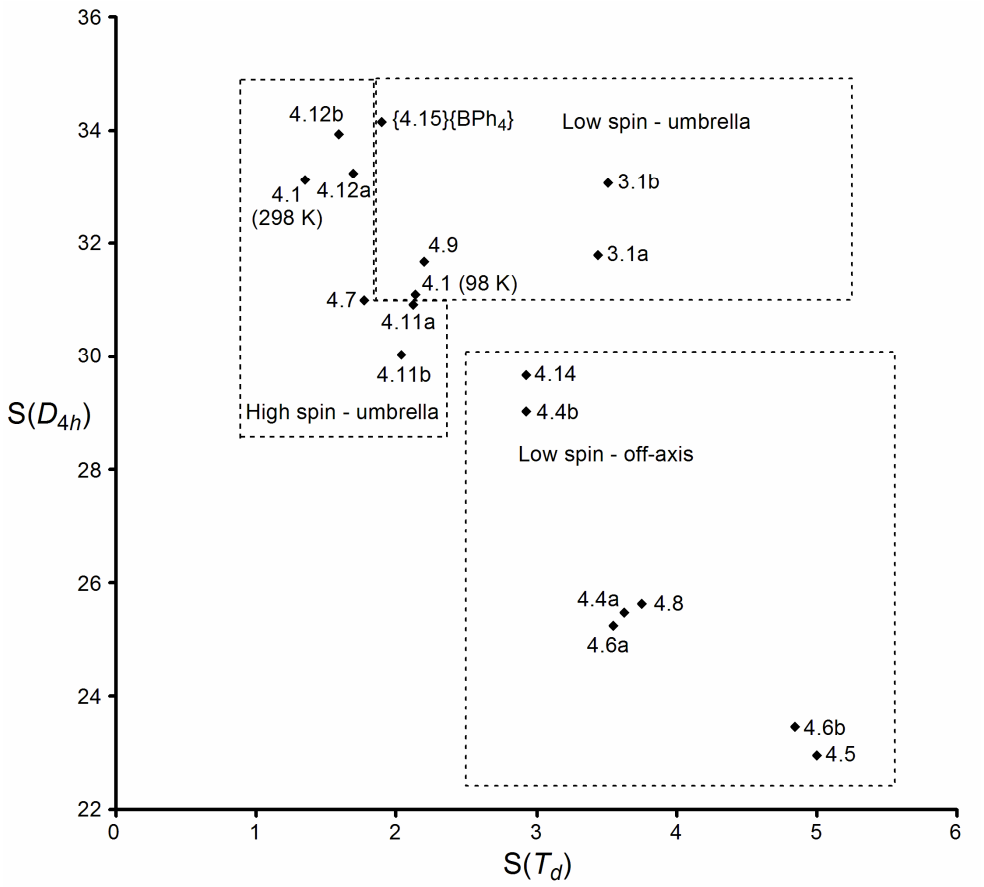

Figure 4.7. The calculated continuous symmetry deviation for each molecule is plotted on a continuous symmetry map of S(T_d) (tetrahedral) versus S(D_{4h}) (square planar). The complexes can be assigned to one of two classes based on their deviations from these two idealized structure types. The umbrella class can be subdivided into high spin and low spin complexes. Complexes with two components on the symmetry map (**a** and **b**) have two asymmetric molecules within the unit cell. The crystal structure of [$PhBP_3$]$CoOSiPh_3$ (**4.1**) was solved at two different temperatures.

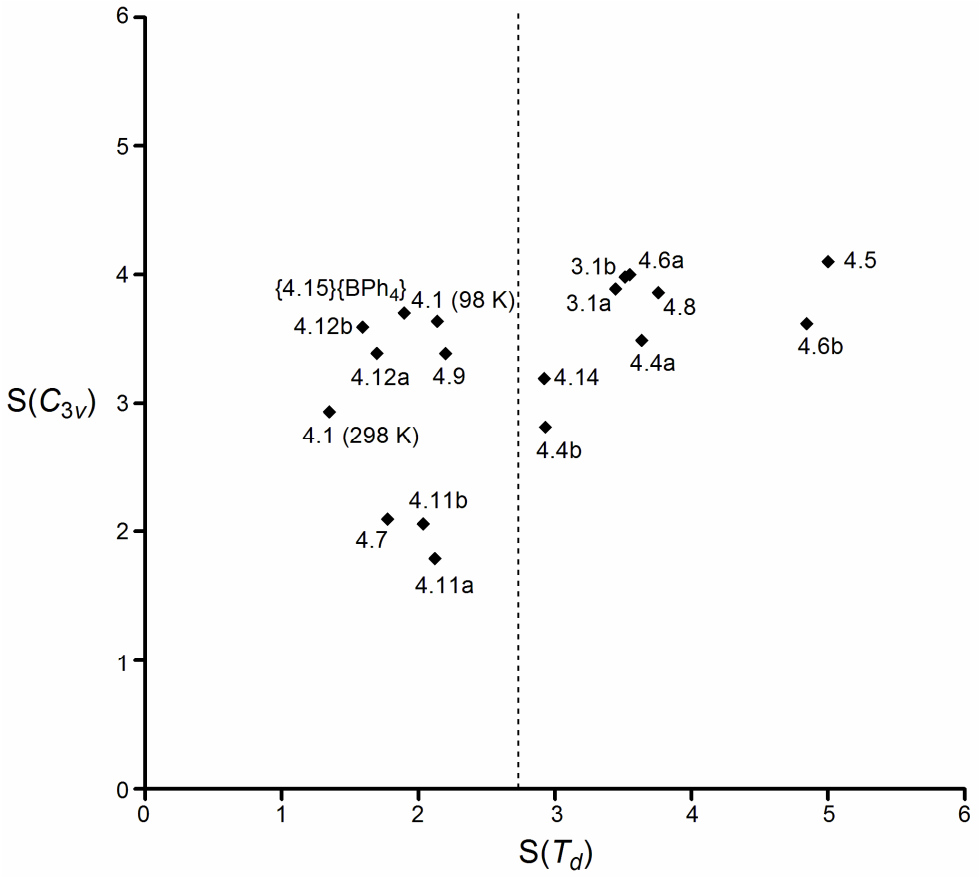

Figure 4.8. The calculated continuous symmetry deviation for each molecule is plotted on a continuous symmetry map of S(T_d) (tetrahedral) versus S(C_{3v}) (trigonal pyramidal). Complexes to the left of the dashed line can be assigned as umbrella distorted while those on the right can be assigned as off-axis distorted. Complexes with two components on the symmetry map (**a** and **b**) have two asymmetric molecules within the unit cell. The crystal structure of [$PhBP_3$]CoOSiPh_3 (**4.1**) was solved at two different temperatures.

Complex **4.2** does not follow the generalized descriptions discussed above since the aryloxide ligand is disordered over two positions, one that exhibits η^1-bonding to the

cobalt center (**4.2**) and one that displays η^3-bonding (**4.2'**) (Figure 4.4).[44] To our knowledge, an η^3-binding mode of an aryloxide ligand is unprecedented for cobalt complexes. In the η^3-bonding mode (**4.2'**), the Co-O bond distance is 1.885(4) Å, and the Co-C bond distances are 2.277(5) and 2.341(5) for C(46) and C(47), respectively. Furthermore, the Co-O-C(46) bond angle is highly bent (88.4(3)°) to accommodate favorable π-bonding to the aryl ring.

Two other solid-state structures are worth discussing in more detail. The solid-state structure determined for diamagnetic {**4.15**}{BPh_4} shows an umbrella distortion (Figure 4.5). The complex is markedly three-fold symmetric and represents an ideal example of structure type **E**, as shown in Figure 4.2. The Co-P distances display a variance of only 0.005 Å, and the average of the three Co-P distances is short at 2.185 Å (Table 4.3). The Co-O bond distance (1.766(3) Å) is only 0.03 Å shorter than in **4.1**, and the Co-O-Si bond angle is almost perfectly linear (178.6(2)°). [$PhBP^{iPr}_3$]$CoSSiPh_3$ (**4.14**) features an off-axis distortion. However, the axial elongation is much more pronounced for complex **4.14** than for the other off-axis complexes. In this case, the axial Co-P bond is greater than 0.17 Å longer than the other two Co-P bonds.

4.2.5 Magnetic characterization (SQUID and EPR) of [BP_3]Co^{II}-X derivatives

As mentioned in the introduction, experimental evidence for the preferred low spin ground state configuration in a L_3Co^{II}-X structure type was first provided by the complex [$PhBP_3$]CoI (**3.1**). In the solid-state this complex displays the distorted structure type represented as **D** in Figure 4.2. The related chloride and bromide complexes [$PhBP_3$]Co-X are also low spin species in their monomeric form in solution, but they give rise to dimeric structures in the crystalline state and are therefore of little utility to the

present discussion. In contrast to these low spin [$PhBP_3$]Co(II) halides, we have previously assigned quartet ground states to the complexes [$PhBP^{iPr}_3$]CoI (**4.12**), [$PhBP^{iPr}_3$]CoCl, and [$PhBP_3$]CoO(2,6-Me_2-Ph) (**3.4**) (type **C** in Figure 4.2). These assignments, considered collectively, suggested to us the possibility that the low and high spin ground states of pseudotetrahedral $L_3Co^{II}X$ structure types may in fact lie closer in energy (i.e., $\Delta H_{HS/LS} = k_BT$) than had been previously anticipated.[15,25]

For the collection of [$PhBP_3$]$Co^{II}X$ complexes presented in this chapter (see Table 4.2) it is clear that a low spin ground state is most typically, though not always, preferred. Moreover, this spin preference is in contrast to Co(II) species supported by the [$PhBP^{iPr}_3$] ligand, where the high spin configuration more typically dominates.

SQUID and EPR data have been collected for all of these [BP_3]Co(II) complexes. Rigorously high spin species include complexes **4.7**, **4.11**, **4.12**, and **4.13**. Each of these complexes adopts a structure that falls into the upper left portion of the symmetry plot shown in Figure 4.7, exhibiting a typical umbrella distortion. Complexes **3.1**, **4.4**, **4.5**, **4.6**, and **4.8** provide examples of rigorously low spin species. The species **4.1**, **4.9**, **4.10**, and **4.14** display spin crossover phenomena in the solid-state. The low spin Co(II) derivatives, type **D** in Figure 4.2, gives rise to stereochemical structures exhibiting both umbrella and off-axis distortions. The interpretation of the magnetic data for **4.2** and **4.3** is more complex due to the potential for η^3 interactions from the X-type ligand.

In examining the [$PhBP_3$] supported thiolates (**4.4**-**4.8**), it is apparent that the preferred ground state is a ^2E. Each complex, excluding **4.7**, has values of $\chi_m T_{av}$ (cm^3 K mol^{-1}) from 10-300 K slightly above the spin only value of $\chi_m T = 0.375$ for a single unpaired electron: **4.4**, 0.41; **4.5**, 0.50; **4.6**, 0.51; **4.8**, 0.45. The solid-state magnetic

moment of complexes **4.4** and **4.6** very gently increases as the temperature of each sample is raised above 250 K. We collected data from 4 K to 300 K, and then back to 4 K for complex **4.6**, and this gentle curvature at higher temperatures is reproducible. It appears likely that partial population of an $S = 3/2$ state is present at higher temperatures. A similar curvature is also observed for [$PhBP_3$]CoI (**3.1**). The low spin thiolates **4.4**, **4.5**, **4.6**, and **4.8** each exhibit an off-axis distortion in the solid-state and short average Co-P bond distances. The EPR data for these three species corroborates their doublet assignments, exhibiting an axial ($g_{\parallel} > g_{\perp}$) EPR signal centered near $g = 2$ (Figure 4.9). On the other hand, complex **4.7** exhibits a $\chi_m T_{av}$ (10-300 K) value of 2.11 cm^3 K mol^{-1} between 10 K and 300 K, an amount that is slightly greater than the spin only value for an $S = 3/2$ system (1.88 cm^3 K mol^{-1}). The low temperature EPR confirms this assignment by showing two signals, one at $g \approx 2$ and a second signal at low field centered at $g \approx 5.8$ (Figure 4.9). The $S = 3/2$ ground state of **4.7** must be due to high steric crowding by the bulky X-type thiolate ligand. Population of the quartet spin state expands the average Co-P bond distances thereby alleviating unfavorable steric contacts.

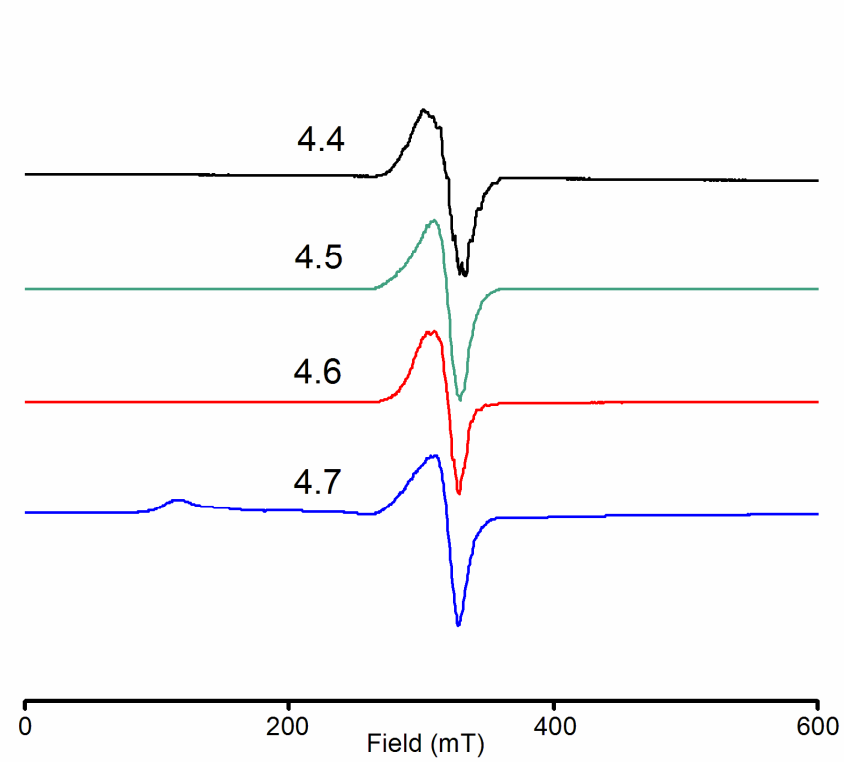

Figure 4.9. Glassy toluene EPR spectra (20 K) of [PhBP$_3$]CoSPh (**4.4**) (—), [PhBP$_3$]CoS(2,6-Me$_2$-Ph) (**4.5**) (—), [PhBP$_3$]CoS(2,4,6-^{i}Pr$_3$-Ph) (**4.6**) (—), and [PhBP$_3$]CoS(2,4,6-^{t}Bu$_3$-Ph) (**4.7**) (—). Instrumental parameters for the spectra can be found in the Experimental Section.

Many pseudotetrahedral Co(II) complexes supported by [Tp] ligands have been prepared, and all of them are high spin.[28,29] Given the preference we have found for [BP$_3$]Co-thiolates to populate low spin ground states, we were curious as to whether a thiolate ligand might confer the low spin configuration to a [Tp]Co(II) system. [Tp]Co thiolates have been prepared previously, and while magnetic data was not reported, they were presumed to be high spin.[33a] We therefore prepared one example of such a complex, [Tp$^{3,5\text{-Me2}}$]CoS(2,6-Me$_2$-Ph) (**4.16**), and obtained low temperature magnetic and structural data to accurately determine a ground spin state (Figure 4.10, see Experimental Section

for synthesis). The SQUID magnetometry data unequivocally shows that **4.16** populates a high spin ground state, with χT_{av} (10 – 300 K) = 2.41 cm^3 K mol^{-1}.

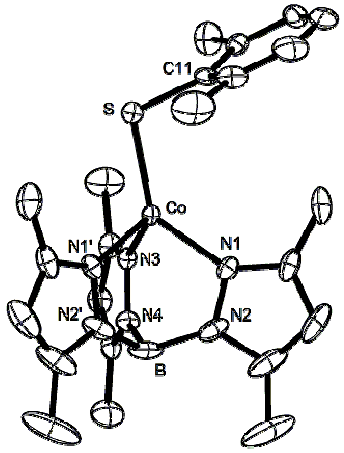

Figure 4.10. Displacement ellipsoid representations (50%) of [$Tp^{3,5\text{-}Me2}$]CoS(2,6-Me_2-Ph), **4.16**. Hydrogen atoms and solvent molecules have been omitted for clarity. Selected interatomic distances (Å) and angles (deg): Co-N1, 2.026(1); Co-N3, 2.021(2); Co-S, 2.273(1); N1-Co-N1', 93.39(8); N1-Co-N3, 93.16(5); N1-Co-S, 134.57(5); N1'-Co-S, 114.07(5); N3-Co-S, 119.04(6).

Whereas thiolate ligands typically confer low spin ground states in the case of [BP_3]Co(II) derivatives, weaker field siloxide ligands form complexes that exhibit spin crossover, as evinced by the complexes [$PhBP_3$]$CoOSiPh_3$ (**4.1**), [$PhBP_3$]CoOSi(4-NMe_2-Ph)$_3$ (**4.9**), and [$PhBP_3$]CoOSi(4-CF_3-Ph)$_3$ (**4.10**). Each of these complexes exhibits an umbrella distortion at low temperature. The structure of **4.1** has been examined both at 98 K (see Figure 4) and at 298 K, and while the average of the Co-P bond distances is expanded at 298 K (reflecting population of the high spin state, vide infra) both X-ray data sets confirm the umbrella distortion (Figure 4.7). Changing

the substituents at the *para* position on the siloxide aryl rings dramatically effects the spin state population at a given temperature (Figure 4.11). The presence of the electron-withdrawing CF_3 group in **4.10** serves to lower the T_c of the spin crossover event. As shown in Figure 4.11, there is a strong temperature dependence of the moment of **4.9**, and a relatively well-defined partial hysteresis is evident centered around 150 K. A more gradual and fully reversible change in $\chi_m T$ is observed above 170 K. This magnetic behavior is distinct from the data collected for **4.1**, which shows gradual crossover (Figure 4.11). EPR spectra were collected at 20 K for **4.1**, **4.9**, and **4.10** and the spectra are consistent with the low temperature SQUID data obtained for each sample.[45] The EPR spectrum of **4.1** shown in Figure 4.12A exhibits an axial signal (g_1 = 2.21, g_2 = 2.05, g_3 = 2.03) featuring well-defined hyperfine coupling (I_{Co} = 7/2) as well as superhyperfine coupling to phosphorus (3 x P, I_P = ½). The observation of phosphorous coupling reflects the highly covalent character of these systems.[46] The octet pattern ($A_{1(Co)}$ = 105 gauss) in the g_1 region of the spectrum suggests a monomeric species in solution (Figure 4.13). Noticeably absent from the spectra of **4.1** and **4.9** are any low field signals that would signify the presence of a high spin Co(II) component.[47] The EPR spectrum of **4.10** (Figure 4.12C) is more interesting. A broad but discernable signal at low field (near g = 5.5) is present at 20 K, suggesting the presence of a high spin component, as is also evident from the solid-state SQUID data. The hyperfine coupling, in the g = 2 region of the spectrum, can be attributed to the presence of the low spin component of **4.10** in the glass, in analogy to the spectra of **4.1** and **4.9**. The effect of solvent in the crystal lattice on the spin crossover process was measured for **4.1** in the solid-state and was found to be minimal.

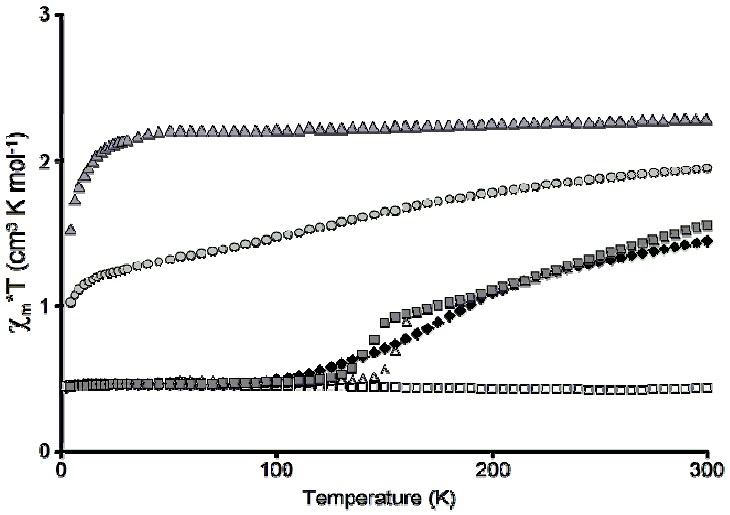

Figure 4.11. SQUID magnetization plot of χ_mT versus T: [PhBP$_3$]CoOSiPh$_3$ (**4.1**) (♦), [PhBP$_3$]CoOSi(4-CF$_3$-Ph)$_3$ (**4.10**) (●), [PhBP$_3$]CoOCPh$_3$ (**4.11**) (▲), [PhBP$_3$]CoSSiPh$_3$ (**4.8**) (□), and [PhBP$_3$]CoOSi(4-NMe$_2$-Ph)$_3$ (**4.9**) as the temperature was raised (Δ) and lowered (■).

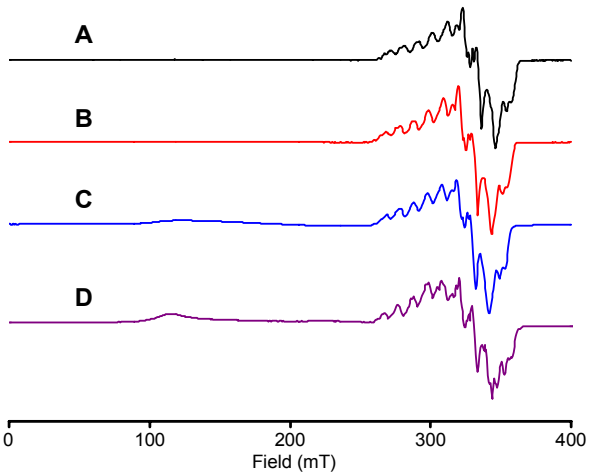

Figure 4.12. Glassy toluene EPR spectra (20 K) for (A) [PhBP$_3$]CoOSiPh$_3$ (**4.1**) (—), (B) [PhBP$_3$]CoOSi(4-NMe$_2$-Ph)$_3$ (**4.9**) (—), (C) [PhBP$_3$]CoOSi(4-CF$_3$-Ph)$_3$ (**4.10**) (—), and (D) [PhBP$_3$]CoOCPh$_3$ (**4.11**) (—). Instrumental parameters for the spectra can be found in the Experimental Section.

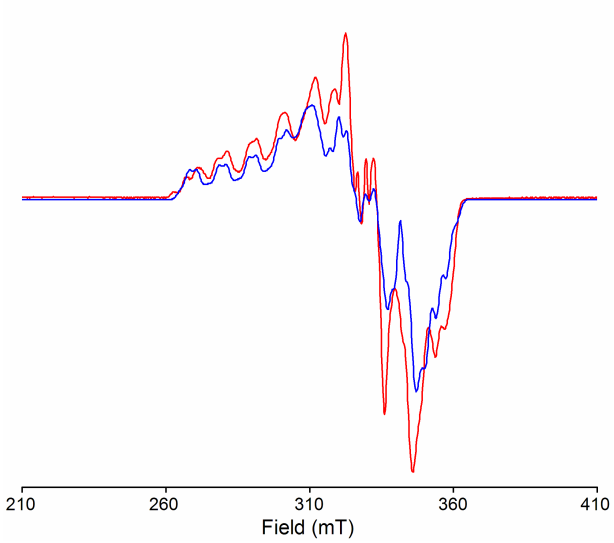

Figure 4.13. Experimental (—) and simulated (—) EPR spectra of $[PhBP_3]CoOSiPh_3$ (**4.1**). Instrumental parameters for the experimental spectrum can be found in the Experimental Section. The simulated parameters are as follows: $g_1 = 2.21$, $g_2 = 2.05$, $g_3 = 2.03$; $a_{1(Co)} = 105$ gauss, $a_{2(Co)} = 12$ gauss, $a_{3(Co)} = 65$ gauss; $a_{1(P)} = 28$ gauss, $a_{2(P)} = 27$ gauss, $a_{3(P)} = 34$ gauss.

Interestingly, the trityloxide complex $[PhBP_3]CoOCPh_3$ (**4.11**) exhibits a highly bent Co-O-C bond angle of 138.0(1)º, compared with the angle of 172.5(1)º for **4.1** and 165.7(1) for related **4.9**. Each of the Co-P bond distances in this umbrella distorted species are also expanded ($Co\text{-}P_{av} = 2.37$ Å). Moreover, each of the Co-P bond distances is expanded ($Co\text{-}P_{av} = 2.37$ Å), suggestive of a high spin ground state in accord with its solid-state SQUID (Figure 4.11) and glassy toluene EPR data (Figure 4.12D).

The magnetic data is complicated for **4.2** and **4.3** due to the possibility of η^3 interactions of the axial ligand. The solid-state crystal structure obtained for **4.2** at 98 K reveals the presence of two distinct conformational isomers. One of these isomers is a four-coordinate pseudotetrahedral species with a $Co\text{-}O\text{-}C_{ipso}$ angle of 110.3(4)º. The other

isomer is nominally five-coordinate and displays an η^3-binding mode of the aryloxide ligand that provides an acute Co-O-C_{ipso} angle of 88.4(3)º. SQUID magnetization data for **4.2** are shown in Figure 4.14. It is clear that the sample predominantly populates a doublet state at low temperature, though a weak signal at low field is discernable in the glassy toluene EPR spectrum of the sample. As the sample is warmed the $\chi_m T$ value gradually rises and at 300 K almost complete crossover to the high spin component is evident. Perhaps the simplest explanation of these data is that the pseudotetrahedral isomer of **4.2** is high spin at all temperatures, and that the isomer that exhibits an η^3-bonding mode is low spin at all temperatures. The magnetic data would then reflect variable populations of the two conformational isomers as a function of temperature in both solid and solution. Consistent with this explanation is the fact that the two other pseudotetrahedral aryloxide and alkoxide complexes we have examined, $[PhBP_3]CoO(2,6\text{-}Me_2\text{-}Ph)$ (**3.4**) and $[PhBP_3]CoOCPh_3$ (**4.11**), both exhibit high spin ground states, and the fact that five-coordinate cobalt(II) systems supported by phosphine ligands invariably populate low spin ground states. The fluorinated aryloxide complex $[PhBP_3]CoO(C_6F_5)$ (**4.3**) is less likely to exhibit π-bonding to the aryl ring due to its electron-withdrawing nature, though interactions with the ortho fluorines of the aryl group cannot be discounted. A similar four-coordinate/five-coordinate equilibrium may explain the change in spin state that is observed in the SQUID data (Figure 4.14).

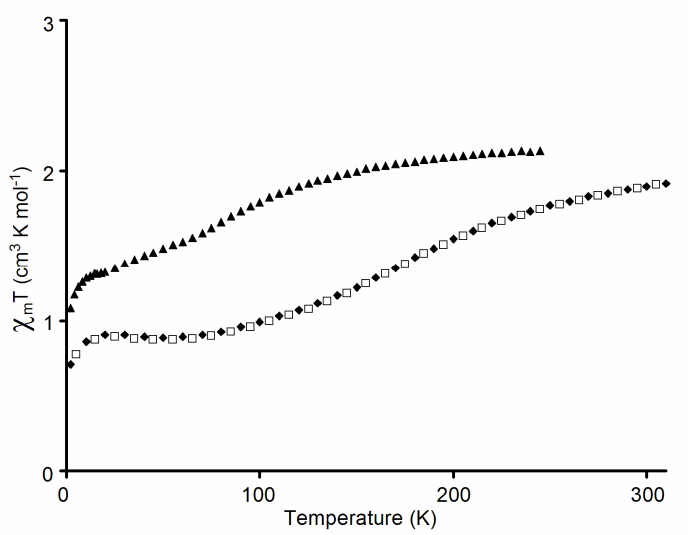

Figure 4.14. SQUID magnetization plot of $\chi_m T$ versus T for [PhBP$_3$]CoO(4-^{t}Bu-Ph) (**4.2**) as the temperature was raised (♦) and then lowered (□), and data for [PhBP$_3$]CoO(C$_6$F$_5$) (**4.3**) (▲) as the temperature was raised.

The complexes supported by the [PhBP$^{i\text{Pr}}_3$] ligand feature two high spin complexes, [PhBP$^{i\text{Pr}}_3$]CoI **(4.12**) and [PhBP$^{i\text{Pr}}_3$]CoOSiPh$_3$ (**4.13**), that exhibit the umbrella distortion, and one thiolate complex, [PhBP$^{i\text{Pr}}_3$]CoSSiPh$_3$ (**4.14**), that exhibits an off-axis distortion and is low spin (vide infra) at low temperature. Structural and magnetic data have been reported previously for [PhBP$^{i\text{Pr}}_3$]CoI (**4.12**). This complex exhibits a high spin ground state configuration and is therefore distinct from its low spin analog [PhBP$_3$]CoI (**3.1**). SQUID data collected on a polycrystalline sample of **4.13** are plotted in Figure 4.15A. The sample is clearly a S = 3/2 system ($\chi_m T_{av}$ (10 K - 300 K) = 2.30 cm^3 K mol^{-1}) and obeys the Curie-Weiss law. Similar magnetic behavior was reported for iodide **4.12**. Magnetization data for the thiolate derivative **4.14** are plotted in Figure 4.15B. The temperature dependence of its magnetic moment is more complex. Below 100 K the sample appears to be low spin ($\chi_m T_{av}$ (10 K - 100 K) = 0.50 cm^3 K

mol^{-1}). A gradual rise in $\chi_m T$ is observed above 100 K and a maximum value of 1.23 cm^3 K mol^{-1} is reached at 300 K, the highest temperature at which the data could be recorded. The magnetic behavior of the sample is fully reversible. The appearance of a gradual spin crossover phenomenon is similar to the rise in magnetic moment that was observed for thiolates **4.4** and **4.6** near room temperature. An interesting observation is that the solution moment of **4.14** at room temperature is 4.0 μ_B, consistent with a fully high spin population. This moment is different from that determined at low temperature by SQUID analysis of the polycrystalline sample, and we therefore elected to further analyze **4.14** by EPR spectroscopy as a powder and as a frozen glass. These data, along with the glassy toluene EPR spectrum of **4.13**, are shown in Figure 4.16. The 20 K glassy toluene spectra of **4.13** and **4.14** (Figure 4.16A and 4.16B) each show spectra characteristic of $S = 3/2$ species. The low field signal present in the glassy spectrum of **4.14** is absent in its powder spectrum at 20 K (Figure 4.16C). There appears therefore to be a stronger preference to populate the high spin configuration in *solution* for this thiolate complex. A different solution conformation of **4.14** may exist than the one that is observed in its solid-state structure at 98 K. Differences in spin behavior between solution and solid samples are not uncommon for spin crossover systems.[48] Even with the stronger donor ligand [$PhBP^{iPr}_3$] these complexes favor the high spin state unless there is a fourth ligand that is an unusually strong donor such as a thiolate ligand. The extreme Co-P axial bond elongation in **4.14** likely reflects a steric compensation that allows the doublet ground state to be populated.

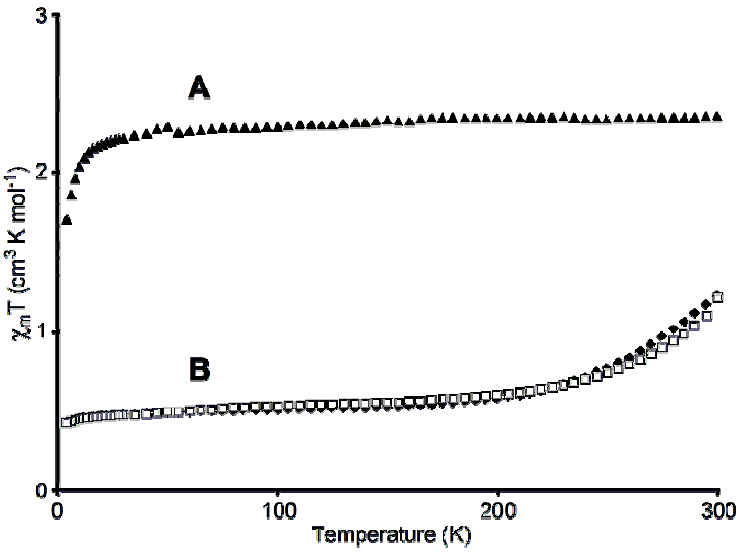

Figure 4.15. SQUID magnetization plot of $\chi_m T$ versus T for (A) [PhBP$^{iPr}_3$]CoOSiPh$_3$ (**4.13**) (▲), and (B) [PhBP$^{iPr}_3$]CoSSiPh$_3$ (**4.14**) as temperature was raised (♦) and then lowered (□).

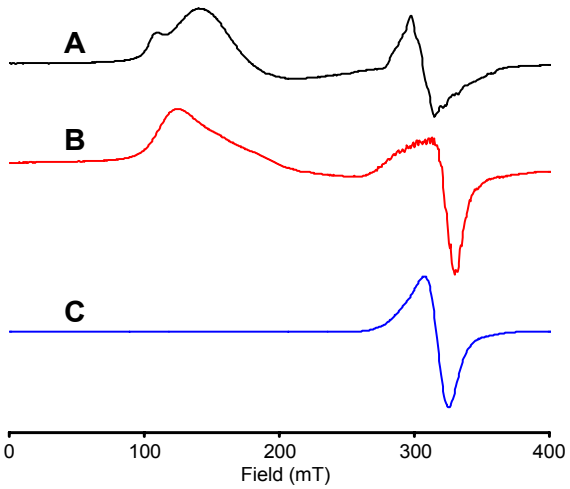

Figure 4.16. Glassy toluene EPR spectra (20 K) of (A) [PhBP$^{iPr}_3$]CoOSiPh$_3$ (**4.13**) (—), and (B) [PhBP$^{iPr}_3$]CoSSiPh$_3$ (**4.14**) (—). Powder sample EPR spectrum (20 K) of (C) [PhBP$^{iPr}_3$]CoSSiPh$_3$ (**4.14**) (—). Instrumental parameters for the spectra can be found in the Experimental Section.

4.2.6 Theoretical analysis of $[BP_3]Co^{II}$-X derivatives

The electronic structure features of umbrella and off-axis geometries share certain similarities, though there are a number of characteristics that distinguish them. To more thoroughly consider the case of their d^7 electronic structures we have undertaken the theoretical DFT examination of one representative complex from each structural subgroup. For this study we chose the siloxide complex $[PhBP_3]CoOSiPh_3$ **4.1** as representative of the umbrella subgroup, and thiolate $[PhBP_3]CoS(2,6\text{-}Me_2\text{-}Ph)$ **4.5** as representative of the off-axis subgroup. Single point electronic structure calculations (DFT) were performed using (i) the experimentally determined X-ray coordinates for each complex as the ground state geometrical structure under (ii) the assumption of a doublet electronic ground state. Each of the structures was subsequently allowed to relax into a theoretically determined global minimum in the absence of geometric constraints, but still under the assumption of a doublet ground state electronic configuration. For each complex, the frontier molecular orbitals obtained by both methods of analysis are qualitatively quite similar. There are, however, noteworthy structural differences between the experimentally and theoretically determined structures.

For pseudotetrahedral **4.1** the predicted frontier molecular orbitals from the geometry-restricted calculation are shown in Figure 4.17. Orbitals calculated for the DFT-optimized structure were calculated and are very similar to those shown here. The singly occupied molecular orbital (SOMO) is energetically well-separated from the lowest unoccupied orbital (LUMO). The lobal representations of the frontier orbitals containing significant d-orbital character map well with those we have sketched qualitatively in Figure 4.2, though the SOMO is predicted by DFT to lie much closer in

energy to the lower set of orbitals than to the LUMO. The SOMO and LUMO orbitals are nearly orthogonal to one another and align reasonably well along the plane containing the Co-O-Si vector. The lowest-lying three orbitals consist of one orbital of dz^2-parentage (HOMO-2) and two orbitals that are canted away from the Co-O-Si vector. While the low symmetry of the structure inevitably gives rise to d-orbital mixing, the lowest-lying pair of orbitals can be very crudely described as *dxy* and dx^2-y^2 type orbitals, where the z-axis is assumed to be coincident with the Co-O-Si vector. Interestingly, there are two high-lying [BP_3]-centered orbitals (HOMO, HOMO-1) comprised within the frontier manifold that would have been difficult to anticipate in the absence of the calculation.

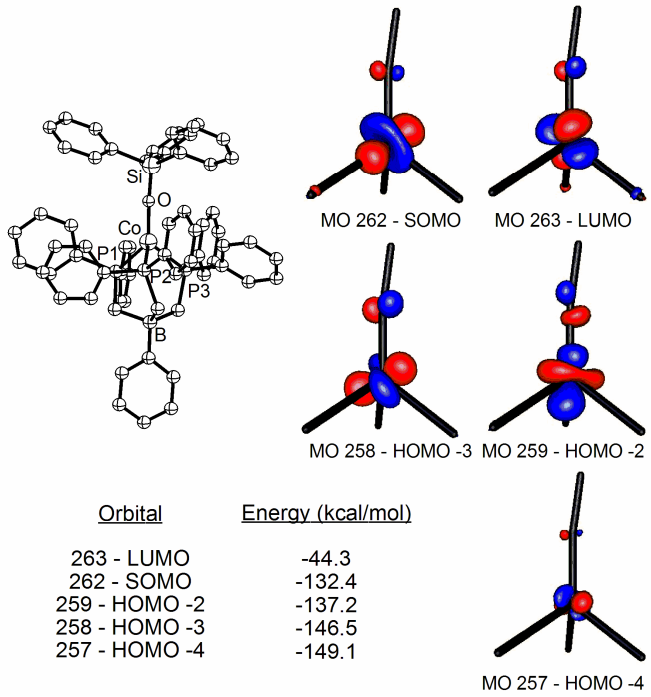

Figure 4.17. Molecular orbitals derived from a single point energy DFT calculation of [$PhBP_3$]$CoOSiPh_3$ (**4.1**) assuming a doublet ground state and the crystallographically determined atomic coordinates.

DFT-minimization of the geometry of **4.1** gives rise to a conformationally similar structure (**4.1**-DFT), with the noteworthy distinction that distortion of one of its Co-P bond distances is grossly exaggerated (2.22 Å, 2.25 Å, 2.43 Å). Despite this structural distinction, the calculation still points to a LUMO that is energetically well-separated from a lower-lying set of d-type orbitals that includes the SOMO. This conclusion is in accord with DFT studies for **4.5**. Table 4.4 compares the core bond lengths and angles of the solid-state structures to the DFT determined structures.

Table 4.4. Experimental and calculated bond lengths and angles for **4.1**, **4.5**, and {**4.15**}.

4.1	Exptl	Calcd	**4.5**	Exptl	Calcd	{**4.15**}	Exptl	Calcd
				Bond Lengths (Å)				
Co-O	1.799	1.849	Co-S	2.167	2.223	Co-O	1.766	1.776
Co-P1	2.156	2.429	Co-P1	2.251	2.418	Co-P1	2.187	2.236
Co-P2	2.284	2.224	Co-P2	2.199	2.271	Co-P2	2.182	2.241
Co-P3	2.169	2.251	Co-P3	2.208	2.286	Co-P3	2.184	2.234
				Bond Angles (deg)				
Co-O-Si	172.5	162.8	Co-S-C46	114.6	119.1	Co-O-Si	178.6	178.7
P1-Co-P2	91.38	88.9	P1-Co-P2	89.44	89.4	P1-Co-P2	90.67	90.8
P1-Co-P3	85.88	94.8	P1-Co-P3	100.23	95.9	P1-Co-P3	90.18	90.8
P2-Co-P3	94.60	88.8	P2-Co-P3	86.73	89.5	P2-Co-P3	90.50	90.5
P1-Co-O	129.45	116.7	P1-Co-S	96.48	99.9	P1-Co-O	125.6	124.4
P2-Co-O	119.42	138.2	P2-Co-S	147.37	145.4	P2-Co-O	124.4	126.4
P3-Co-O	125.82	118.1	P3-Co-S	123.30	122.1	P3-Co-O	124.8	123.5

Lobal representations of the frontier molecular orbitals of the off-axis thiolate complex **4.5** based upon a single-point electronic structure calculation are displayed in Figure 4.18. The LUMO is again energetically well-separated from a set of low-lying d-type orbitals. Certain comparative differences do arise with respect to the MO structure of **4.1**. The LUMO now appears to be coincident with the trigonal plane defined by two Co-P vectors and the Co-S vector, and the SOMO is directed with a lobe that is pointed towards the axial P donor ligand. The shape of the SOMO explains why the axial phosphine ligand is appreciably elongated in the crystal structure of **4.5**. The DFT-minimized structure, **4.5**-DFT, dramatically exaggerates this elongation, as was also observed for the case of **4.1**. The HOMO and HOMO-1 orbitals are no longer ligand centered but now comprise d-type orbitals with additional contributions from the equatorial thiolate ligand. The phasing suggests that the interaction is of Co-S π^* character in each case. The lowest-lying orbital is difficult to distinguish from the HOMO and HOMO-1 orbitals, and the high degree of mixing due to the low symmetry of the system is evident.

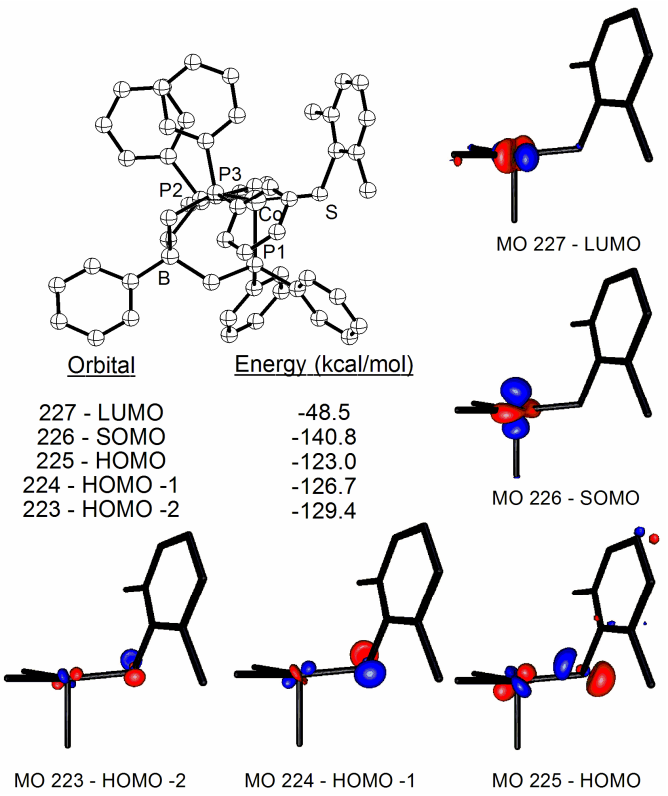

Figure 4.18. Molecular orbitals derived from a single point energy DFT calculation of [PhBP$_3$]CoS(2,6-Me$_2$-Ph) (**4.5**) assuming a doublet ground state and the crystallographically determined atomic coordinates.

The transition state for dissociation of one phosphine ligand should look similar to the highly distorted structures we have calculated for **4.1** and **4.5**. In this context it is interesting to note that the d^7 low spin half-sandwich complex [Tp]Co[Cp*] has been characterized, and dissociation of one of its pyrazolyl donor arms is indeed observed in the solid-state.[9e,f] The authors have suggested that in solution an equilibrium between the κ^2- and κ^3-binding modes is present.[9f] The crystal structure of **4.14** is interesting for comparison in that it provides an experimentally determined ground state structure featuring one Co-P bond that is strikingly elongated by comparison to the other two. In effect, the crystal structure of this complex is a better match for the theoretical structure

obtained for **4.5**, and related d^7 $[BP_3]Ni(NR)$ species, by virtue of the exaggerated distortion.[49] Because the solution magnetic (Evans) and EPR data for **4.15** are indicative of a high spin component, it is reasonable to suggest that an equilibrium mixture between κ^2- and κ^3-binding modes might exist in solution. Nevertheless, it seems more likely to us that the equilibrium is between an umbrella distorted high spin structure, similar to **4.7**, and an off-axis distorted low spin structure in the solid-state.

Our inability to faithfully reproduce the crystallographically determined structures of **4.1** and **4.5** detracts from our confidence to use DFT methods to theoretically predict the ground spin-state of these systems. To illustrate this point, when we calculate the total energy of the DFT-minimized structures of iodide **3.1** assuming a doublet and a quartet state, respectively, the quartet state is energetically favored by 8.8 kcal/mol. This result is in obvious contradiction to the experimentally observed low spin state preference. A general problem associated with open-shell DFT calculations is that there is, as yet, no universally applicable method and basis-set that can be confidently applied to a given system.

The geometries and electronic structures of closed-shell coordination complexes are more reliably predicted by current DFT methods, and we therefore examined diamagnetic $\{\mathbf{4.15}\}^+$. The nature of the SOMO orbital of **4.1** suggests that the removal of one unpaired electron should relieve its distorted structure. This is in fact observed, both crystallographically and theoretically. Recall that XRD analysis of $\{\mathbf{4.15}\}\{BPh_4\}$ revealed an extremely symmetric structure containing a P_3Co subunit defining one half of an octahedron almost perfectly trisected by the Co-O-Si bond vector (Figure 4.5). Complex $\{\mathbf{4.15}\}^+$ can be consequently classified by structure type **E** from Figure 4.2, and

its molecular orbital diagram is therefore anticipated to reflect the two-over-three splitting diagram of an octahedral complex. The presence of degenerate π-binding should give rise to a sizable separation between the upper two and lower three d-orbitals. This picture is evident from the single-point electronic structure calculation performed for {**4.15**}$^{+}$. Lobal representations for the orbitals of dominant d-type contributions are shown in Figure 4.19. As for the MO structure of **4.1**, a number of filled ligand centered orbitals lie at relatively high energy, in this case falling between the lower-lying (a_1 + e) filled d-orbital set comprised of dz^2, *dxy*, and dx^2-y^2 and the upper-lying, empty d-orbital e set comprising *dxz* and *dyz*. These frontier d-orbitals reflect the unmistakable analogy between pseudotetrahedral {**4.15**}$^{+}$ and the electronic structure of sandwich and half-sandwich complexes.[9f,50] The DFT-optimized structure for {**4.15**}$^{+}$ was found to be in good agreement with the crystal structure of {**4.15**}{BPh_4} (Table 4.4).

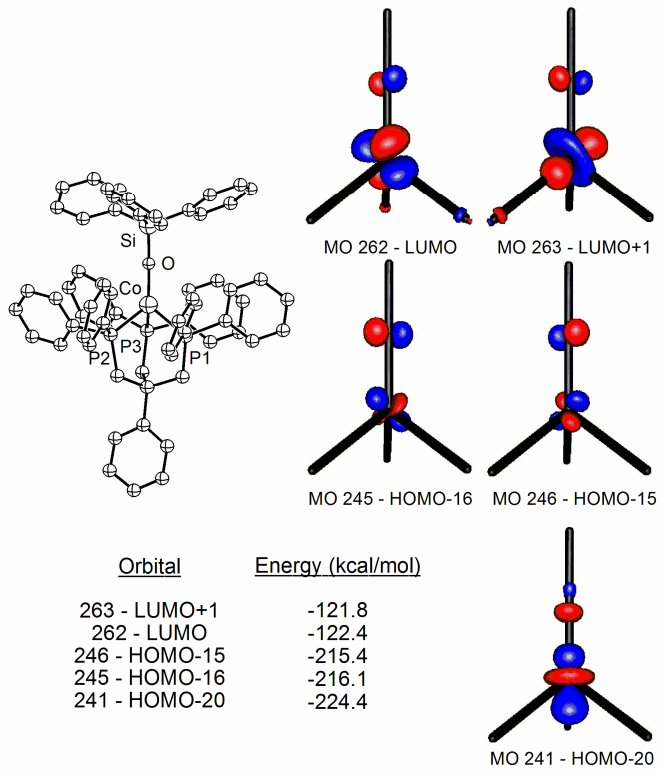

Figure 4.19. Molecular orbitals consisting of significant d-orbital contributions for the frontier region of $\{\mathbf{4.15}\}^{+}$. Orbitals were derived from a single-point electronic structure calculation assuming a singlet ground state and the crystallographically determined atomic coordinates.

4.3 Conclusion

It is evident from the present study that magnetic phenomena for distorted tetrahedral d^7 ions can be much richer then had been appreciated previously. For highly covalent $[BP_3]Co(II)$ complexes, low spin, high spin, and spin crossover complexes are readily accessible for a variety of related geometries best described as pseudotetrahedral with an umbrella or off-axis distortion. The observation of an $S = ½$ ground state for tetracoordinate $[BP_3]Co^{II}X$ complexes appears at this stage to be neither exceptional nor

uncommon–a host of such complexes have now been thoroughly characterized. Given this situation, it is of obvious interest to re-examine other d^7 L_3CoX scaffolds to determine whether access to the $S = ½$ ground state will prove more ubiquitous than was previously thought. Tetracoordinate L_3Co^{II}-SR thiolate complexes should offer a good starting point in this regard, though for the single [Tp]Co(II) thiolate we have examined, the more typical $S = 3/2$ ground state is preferred.

Our data establish that ground spin-state assignments for these types of d^7 ions can be readily made by inspection of their low-temperature solid-state structural, SQUID, and EPR data. The halide structures $[PhBP_3]CoI$ and $[PhBP^{iPr}_3]CoCl$ represent the simplest limiting cases.[15,25] For example, the crystal structure of $[PhBP_3]CoI$ reveals its $S = ½$ ground state by virtue of its three relatively short Co-P distances, with one bond longer than the other two. This contrasts with the structure of $[PhBP^{iPr}_3]CoCl$, in which each Co-P distance is elongated but essentially equidistant, and a threefold axis is more readily discerned. The collection of low temperature data collected for complexes **4.2** and **4.3** serve as a reminder that SQUID or EPR data need to be interpreted cautiously in the absence of structural data. In particular, slippage of a monodentate X-type ligand to a higher coordination mode (e.g., from η^1 to η^3) can confer a spin-state change.

Curious and perhaps still counterintuitive is that the stronger-field donor ligand $[PhBP^{iPr}_3]$ tends to confer the high spin configuration. Such is the case not only for $[PhBP^{iPr}_3]CoCl$, but also for $[PhBP^{iPr}_3]CoI$ (**4.12**) and $[PhBP^{iPr}_3]CoOSiPh_3$ (**4.13**). To account for this, we maintain that conformational constraints imposed by the $[PhBP^{iPr}_3]$ ligand will disfavor short Co-P contacts so as to minimize steric repulsion by the isopropyl groups of this bulky ligand. In the absence of overriding factors, such as strong

π-bonding at the X-linkage, a high spin population is energetically preferred. By choosing a more strongly π-donating X-type linkage, as is the case for the complex [PhBP$^{i\text{Pr}}_3$]CoSSiPh$_3$ (**4.14**), an S = ½ ground state can be realized (at least in the solid-state), but now the requisite distortion that relieves the σ* (and appreciably π*) interaction of the SOMO is far more pronounced than for the case of low spin [PhBP$_3$] systems.

While these examples illustrate the effect that rather dramatic structural and electronic differences can have on the observed ground spin-states of these systems, more subtle differences can have equally striking consequences. For instance, the complex [PhBP$_3$]CoS(2,4,6-^{i}Pr$_3$-Ph) (**4.6**) is an off-axis low spin species, whereas [PhBP$_3$]CoS(2,4,6-^{t}Bu$_3$-Ph) (**4.7**) adopts a distinctly different umbrella distortion and populates a high spin ground state. Even more subtle changes can have profound electronic consequences. Replacement of the trityl C-atom in [PhBP$_3$]CoOCPh$_3$ (**4.11**) by the Si-atom in [PhBP$_3$]CoOSiPh$_3$ (**4.1**) alters the system's ground electronic state from S = 3/2 to S = ½, respectively. This secondary sphere effect is striking and is immediately evident by comparison of the low temperature glassy toluene EPR spectra of the two samples. We have also shown that the spin population of a d^7 L$_3$CoX system can be fine-tuned by adjusting the electron-donor character of the X-type linkage at a site even further removed from the cobalt center. This possibility is evident from the SQUID magnetization and EPR data for [PhBP$_3$]CoOSi(4-NMe$_2$-Ph)$_3$ (**4.9**) and [PhBP$_3$]CoOSi(4-CF$_3$-Ph)$_3$ (**4.10**) and, moreover, suggests that truly cooperative spin crossover d^7 L$_3$CoX platforms might be realized if X-type linkages can be appropriately tailored. This possibility represents an exciting opportunity, as it would enable the

reactivity patterns of structurally related $S = 1/2$ and $S = 3/2$ coordinatively unsaturated d^7 ions to be probed as a function of their spin populations.[32c,51]

4.4 Experimental section

4.4.1 General considerations

General procedures were performed according to Section 2.4.1 and 3.5.1. Magnetic measurements were conducted as described in Section 3.5.2. EPR measurements and simulations were conducted as described in Section 3.5.3.

4.4.2 EPR measurements

Table 4.5. Instrumental parameters for the EPR spectra shown.

Complex Number	**4.1**	**4.2**	**4.3**	**4.4**	**4.5**	**4.6**	**4.7**
Solvent	toluene	toluene	toluene	toluene	toluene	toluene	toluene
Temperature (K)	20	20	20	77	77	10	20
ν (GHz)	9.475	9.474	9.380	9.380	9.379	9.378	9.379
Modulation frequency (kHz)	100	100	100	100	100	100	100
Modulation amplitude (gauss)	4	5	4	4	4	4	4
Microwave power (mW)	0.202	2.02	2.02	0.641	2.02	0.638	2.02
Conversion time (ms)	81.92	81.92	81.92	163.84	81.92	81.92	81.92
Time constant (ms)	20.48	20.48	20.48	40.96	20.48	20.48	20.48
Scans	2	4	3	1	2	1	3

Table 4.5. (cont.)

Complex Number	**4.8**	**4.9**	**4.10**	**4.11**	**4.13**	**4.14**	**4.14**
Solvent	toluene	toluene	toluene	toluene	toluene	toluene	powder
Temperature (K)	20	20	20	20	20	20	20
ν (GHz)	9.380	9.378	9.378	9.379	9.377	9.378	9.382
Modulation frequency (kHz)	100	100	100	100	100	100	100
Modulation amplitude (gauss)	4	4	4	4	4	4	4
Microwave power (mW)	0.638	0.0639	0.00639	0.202	0.639	0.638	0.0638
Conversion time (ms)	81.92	81.92	81.92	81.92	81.92	81.92	81.92
Time constant (ms)	20.48	20.48	20.48	20.48	20.48	20.48	20.48
Scans	1	1	1	1	1	1	3

4.4.3 Computational methods

All calculations were performed using the hybrid DFT functional B3LYP as implemented in the Jaguar 5.0 program package.[52] This DFT functional utilizes the Becke three-parameter functional[53] (B3) combined with the correlation functional of Lee, Yang, and Parr[54] (LYP). LACVP** was used as the basis set. Input coordinates were derived as described in the text from crystallographically determined structures. Spin-states and molecular charges were explicitly stated, and no molecular symmetry was imposed. Default values for geometry and SCF iteration cutoffs were used. All structures

converged under these criteria except for the geometry minimization of **4.1**. In this case, multiple additional cycles showed no more than 1 kcal/mol difference in energy.

The continuous symmetry measurements were determined with the program SHAPE developed at the Universitat de Barcelona, Spain.[55]

4.4.4 Starting materials and reagents

The preparation of [$PhBP_3$]CoI (**3.1**) and ([$PhBP_3$]CoCl) (**3.3**) is described in Chapter 3. [$PhBP^{iPr}_3$]CoI (**4.12**) was prepared according to a literature procedure. The reagents $TlOSiPh_3$,[56] TlO-*p*-^{t}Bu-Ph, TlSPh,[57] HS(2,4,6-^{i}Pr_3-Ph),[58] HS(2,4,6-^{t}Bu_3-Ph),[59] HOSi(*p*-NMe_2-Ph)$_3$,[60] HOSi(*p*-CF_3-Ph)$_3$,[61] {[Cp]$_2$Fe}{BPh_4},[62] and {[Cp]$_2$Fe}{B(3,5-$(CF_3)_2$-Ph)$_4$}[63] were prepared according to literature procedures. TlO(C_6F_5), TlS(2,6-Me_2-Ph), TlS(2,4,6-^{i}Pr_3-Ph), TlS(2,4,6-^{t}Bu_3-Ph), $TlSSiPh_3$, $TlOCPh_3$, TlOSi(*p*-NMe_2-Ph)$_3$, and TlOSi(*p*-CF_3-Ph)$_3$ were prepared via a modification of a general synthetic method reported by Tolman (see below). The reagents HO(*p*-^{t}Bu-Ph), HO(C_6F_5), HSPh, HS(2,6-Me_2-Ph), $HOCPh_3$, $HOSiPh_3$, $HSSiPh_3$, $CoBr_2$, and [K][$Tp^{3,5\text{-}Me2}$] were purchased from commercial vendors and used without further purification. Thallium ethoxide was purchased from Aldrich, filtered through a pad of Celite to remove insoluble black material, and then stored at -35 °C.

General method for the preparation of thallium reagents (modified from Tolman et. al.): The appropriate phenol, thiol, silanol, or silylthiol (about 200 mg) was dissolved in petroleum ether (10 mL) and a minimal amount of THF (if necessary). One equivalent of thallium ethoxide was added as a petroleum ether solution (4 mL), and the reaction mixture was stirred for 30 min. The reaction was preformed in the dark to minimize thallium ethoxide degradation. The precipitates were collected on a medium frit

and washed with petroleum ether (2 x 10 mL) and then dried. The thallium reagents were used without further purification.

4.4.5 Synthesis of compounds

Additional ^{1}H NMR data for [PhBP$_3$]CoI, 3.1. ^{1}H NMR (C_6D_6, 300 MHz): δ 22.3 (6 H, T_1 = 2.4 ms, PhB(C*H*$_2$PPh$_2$)$_3$), 10.8 (12 H, T_1 = 23.6 ms, *meta* P(C$_6$*H*$_5$)$_2$), 7.7 (2 H, T_1 = 40.5 ms, *ortho* B(C$_6$*H*$_5$)), 7.5 (3 H, T_1 = 205 ms, *meta* and *para* B(C$_6$*H*$_5$)), 4.3 (12 H, T_1 = 1.2 ms, *ortho* P(C$_6$*H*$_5$)$_2$), 2.2 (6 H, T_1 = 46.7 ms, *para* P(C$_6$*H*$_5$)$_2$).

Synthesis of [PhBP$_3$]CoOSiPh$_3$, 4.1. A THF (4 mL) solution of TlOSiPh$_3$ (0.173 g, 0.361 mmol) was added dropwise to a stirring solution of [PhBP$_3$]CoI (**3.1**) (0.315 g, 0.361 mmol) in THF (8 mL). The resulting solution was allowed to stir for 10 h. An orange precipitate formed (TlI), which was filtered away over diatomaceous earth. The THF was then removed in vacuo and the resulting solid was dissolved in benzene (4 mL). Crystals were grown via vapor diffusion of petroleum ether into a benzene solution. The purple crystals were dried and weighed (0.300 g, 81% yield). The crystals were recrystallized two additional times (from benzene/petroleum ether) before measurements were taken on the samples (95% yield for each recrystallization). ^{1}H NMR (C_6D_6, 300 MHz): δ 15.6, 10.0, 9.8, 8.6, 8.3, 7.4, 1.1 (br), -2.2. ^{1}H NMR (d$_8$-toluene, 300 MHz): δ 15.4, 9.9, 9.7, 8.6, 8.1, 7.4 (m), 7.1 (m), 1.1 (br), -2.0. UV-vis (C_6H_6) λ_{max}, nm (ε): 557 (700), 763 (310). UV-vis (C_6D_6) λ_{max}, nm (ε): 557 (670), 757 (280), 1136 (320). UV-vis (toluene) λ_{max}, nm (ε): 557 (650), 763 (290). UV-vis (THF) λ_{max}, nm (ε): 557 (670), 761 (300). Evans Method (C_6D_6 – 295 K): 3.42 μ_B; (d$_8$-toluene – 295 K): 3.51 μ_B; (d$_8$-THF – 295 K): 3.54 μ_B. EPR (toluene, 20 K): g_x = 2.03, $a_{x(Co)}$ = 65 gauss, $a_{x(P)}$ = 34 gauss; g_y = 2.05, $a_{y(Co)}$ = 12 gauss, $a_{y(P)}$ = 27 gauss; g_z = 2.21, $a_{z(Co)}$ = 105 gauss, $a_{z(P)}$ = 28 gauss.

Electrochemistry (vs. ferrocene in THF with [TBA][ClO_4] as supporting electrolyte): Co^{II}/Co^{III}, -360 mV; Co^{I}/Co^{II}, -1290 mV. Anal. Calcd for $C_{63}H_{56}BCoOP_3Si$: C, 74.19; H, 5.53. Found: C, 74.27; H, 5.42.

Synthesis of [$PhBP_3$]CoO(4-^{t}Bu-Ph), 4.2. Followed protocol for **4.1**. Used TlO-*p*-^{t}BuPh (85.8 mg, 0.243 mmol) and **3.1** (212 mg, 0.243 mmol). Red-brown crystals of **4.2** were isolated (115 mg, 53% yield). ^{1}H NMR (C_6D_6, 300 MHz): δ 12.3 (br), 9.2, 7.7, 2.1, 1.2, 0.9, 0.5 (br). UV-vis (C_6H_6) λ_{max}, nm (ε): 428 (2300), 567 (1600), 715 (700). Evans Method (C_6D_6): 3.43 μ_B. Electrochemistry (vs. ferrocene in THF with [TBA][PF_6] as supporting electrolyte): Co^{II}/Co^{III}, -390 mV; Co^{I}/Co^{II}, -1330 mV. Anal. Calcd for $C_{55}H_{54}BCoOP_3$: C, 73.92; H, 6.09. Found: C, 73.58; H, 6.01.

Synthesis of [$PhBP_3$]CoO(C_6F_5), 4.3. Followed protocol for **4.1**. Used TlO(C_6F_5) (109 mg, 0.281 mmol) and **3.1**, (245 mg, 0.281 mmol). Olive green crystals of **4.3** were isolated (159 mg, 59% yield). ^{1}H NMR (C_6D_6, 300 MHz): δ 16.9, 10.9, 8.5, 7.5, -1.0, -3.4, -61.8. ^{19}F NMR (C_6D_6, 282 MHz): δ -73.1, -181.0. UV-vis (C_6H_6) λ_{max}, nm (ε): 582 (740), 712 (560). Evans Method (C_6D_6): 3.8 μ_B. Anal. Calcd for $C_{51}H_{41}BCoF_5OP_3$: C, 66.04; H, 4.46. Found: C, 65.19; H, 4.39.

Synthesis of [$PhBP_3$]CoSPh, 4.4. Followed protocol for **4.1**. Used TlSPh (94.0 mg, 0.300 mmol) and **3.1** (261 mg, 0.300 mmol). Red crystals of **4.4** were isolated (193 mg, 75% yield). ^{1}H NMR (C_6D_6, 300 MHz): δ 24.7 (br), 16.7, 10.7, 8.3, 7.7, 7.6, 2.2 (br), 1.4, -3.1 (br), -6.0. UV-vis (C_6D_6) λ_{max}, nm (ε): 460 (3500), 597 (1800), 1204 (270). Evans Method (C_6D_6): 2.43 μ_B. Electrochemistry (vs. ferrocene in THF with [TBA][PF_6] as supporting electrolyte): Co^{II}/Co^{III}, -160 mV; Co^{I}/Co^{II}, -1120 mV. Anal. Calcd for $C_{51}H_{46}BCoP_3S$: C, 71.76; H, 5.43. Found: C, 71.94; H, 5.42.

Synthesis of [PhBP$_3$]CoS(2,6-Me$_2$-Ph), 4.5. Followed protocol for **4.1**. Used TlS(2,6-Me$_2$-Ph) (102 mg, 0.297 mmol) and **3.1** (259 mg, 0.297 mmol). Red crystals of **4.5** were isolated (172 mg, 66% yield). ^{1}H NMR (C_6D_6, 300 MHz): δ 79.8, 26.7, 19.6, 13.1, 9.9, 8.2, 8.0, 0.5 (br), -1.1, -21.1. UV-vis (C_6H_6) λ_{max}, nm (ε): 396 (4600), 486 (3200), 599 (2300), 741 (900). Evans Method (C_6D_6): 2.28 μ_B. Electrochemistry (vs. ferrocene in THF with [TBA][ClO_4] as supporting electrolyte): Co^{II}/Co^{III}, -170 mV; Co^{I}/Co^{II}, -1100 mV. Anal. Calcd for $C_{53}H_{50}BCoP_3S$: C, 72.20; H, 5.72. Found: C, 72.42; H, 5.69.

Synthesis of [PhBP$_3$]CoS(2,4,6-^{i}Pr$_3$-Ph), 4.6. Followed protocol for **4.1**. Used TlS(2,4,6-^{i}Pr$_3$-Ph) (117 mg, 0.265 mmol) and {[PhBP$_3$]CoCl} (**3.3**) (207 mg, 0.265 mmol). Red-brown crystals of **4.6** were isolated (178 mg, 68% yield). ^{1}H NMR (C_6D_6, 300 MHz): δ 46.4 (br), 21.7, 11.6, 9.1, 8.9, 7.8, 7.7, 4.8, 1.3, 0.9. UV-vis (C_6H_6) λ_{max}, nm (ε): 384 (6600), 471 (4200), 609 (3000), 743 (900). Evans Method (C_6D_6): 2.80 μ_B. Electrochemistry (vs. ferrocene in THF with [TBA][PF_6] as supporting electrolyte): Co^{II}/Co^{III}, -80 mV; Co^{I}/Co^{II}, -1190 mV. Anal. Calcd for $C_{60}H_{64}BCoP_3S$: C, 73.54; H, 6.58. Found: C, 73.18; H, 6.57.

Synthesis of [PhBP$_3$]CoS(2,4,6-^{t}Bu$_3$-Ph), 4.7. Followed protocol for **4.1**. Used TlS(2,4,6-^{t}Bu$_3$-Ph) (145 mg, 0.302 mmol) and **3.1** (263 mg, 0.302 mmol). Red crystals of **4.7** were isolated (113 mg, 36% yield). ^{1}H NMR (C_6D_6, 300 MHz): δ 50.8, 16.7, 12.8, 10.6 (br), 9.2, 8.1, 2.3, -3.2 (br), -5.4, -27.0. UV-vis (C_6D_6) λ_{max}, nm (ε): 479 (3600), 640 (1900), 754 (1800), 1190 (430). Evans Method (C_6D_6): 3.90 μ_B. Electrochemistry (vs. ferrocene in THF with [TBA][PF_6] as supporting electrolyte): Co^{II}/Co^{III}, -60 mV;

Co^{I}/Co^{II}, -1080 mV. Anal. Calcd for $C_{63}H_{70}BCoP_3S$: C, 74.04; H, 6.90. Found: C, 73.95; H, 6.98.

Synthesis of [PhBP$_3$]CoSSiPh$_3$, 4.8. Followed protocol for **4.1**. Used $TlSSiPh_3$ (187 mg, 0.376 mmol) and **3.1** (328 mg, 0.376 mmol). Green crystals of **4.8** were isolated (321 mg, 83% yield). ^{1}H NMR (C_6D_6, 300 MHz): δ 46.4, 11.9, 8.7-6.6, 1.3. UV-vis (C_6H_6) λ_{max}, nm (ε): 622 (1300), 747 (670). Evans Method (C_6D_6): 2.53 μ_B. Electrochemistry (vs. ferrocene in THF with [TBA][PF_6] as supporting electrolyte): Co^{II}/Co^{III}, -210 mV (irreversible), Co^{I}/Co^{II}, -1010 mV. Anal. Calcd for $C_{63}H_{56}BCoP_3SSi$: C, 73.04; H, 5.45. Found: C, 73.06; H, 5.49.

Synthesis of [PhBP$_3$]CoOSi(4-NMe$_2$-Ph)$_3$, 4.9. Followed protocol for **4.1**. Used $TlOSi(p\text{-}NMe_2\text{-}Ph)_3$ (228 mg, 0.374 mmol) and ([$PhBP_3$]CoCl) (**3.3**) (292 mg, 0.374 mmol). Layering of petroleum ether (14 mL) onto a toluene solution (4 mL) afforded red crystalline product (173 mg). The recrystallization of the product from the supernatant leads to additional product (115 mg) to give a total yield of 67%. ^{1}H NMR (C_6D_6, 300 MHz): δ 103.7, 14.6, 10.1 (br), 9.5, 8.1, 7.8, 7.4, 2.7, 2.1, -1.0. UV-vis (C_6H_6) λ_{max}, nm (ε): 555 (940), 699 (440), 772 (420). Evans Method (C_6D_6): 3.46 μ_B. Electrochemistry (vs. ferrocene in THF with [TBA][ClO_4] as supporting electrolyte): Co^{II}/Co^{III}, -360 mV; Co^{I}/Co^{II}, -1300 mV. Anal. Calcd for $C_{69}H_{71}BCoN_3OP_3Si$: C, 72.12; H, 6.23; N, 3.66. Found: C, 71.77; H, 6.40; N, 3.52.

Synthesis of [PhBP$_3$]CoOSi(4-CF$_3$-Ph)$_3$, 4.10. Followed protocol for **4.1**. Used $TlOSi(p\text{-}CF_3\text{-}Ph)_3$ (99 mg, 0.145 mmol) and ([$PhBP_3$]CoCl) (**3.3**), (113 mg, 0.145 mmol). The toluene solution (2 mL) was layered with 15 mL of petroleum ether and cooled to -35 ºC until crystals formed. The crystals were then dried in vacuo yielding the pure

compound (117 mg, 66% yield). ^{1}H NMR (C_6D_6, 300 MHz): δ 17.4, 10.7, 9.8 (br), 8.8, 8.5, 7.3, -0.9, -4.2, -81.6 (br). ^{19}F NMR (C_6D_6, 282 MHz): δ -58.1. UV-vis (C_6H_6) λ_{max}, nm (ε): 560 (740), 757 (320). Evans Method (C_6D_6, 298 K): 3.93 μ_B. Electrochemistry (vs. ferrocene in THF with [TBA][ClO_4] as supporting electrolyte): Co^{II}/Co^{III}, -60 mV (irreversible), Co^{I}/Co^{II}, -1080 mV. Anal. Calcd for $C_{66}H_{53}BCoF_9OP_3Si$: C, 64.77; H, 4.36. Found: C, 64.70; H, 4.55.

Synthesis of [PhBP$_3$]CoOCPh$_3$, 4.11. A THF solution (3 mL) of the thallium reagent $TlOCPh_3$ (124 mg, 0.267 mmol) was added to a stirring THF solution (10 mL) of [$PhBP_3$]CoI, **3.1** (233 mg, 0.267 mmol). The solution was stirred for 4 h and a yellow precipitate formed (TlI). The precipitate was removed by filtration over diatomaceous earth. The remaining reaction volatiles were removed in vacuo, and the blue-green powder was then washed with petroleum ether (2 x 10 mL) and dried. The solid was then redissolved in benzene (4 mL) and then triturated with petroleum ether (15 mL). The supernatant was separated from the brown solid via filtration. The blue-green solution was dried in vacuo and then crystallized by vapor diffusion of petroleum ether into a benzene solution (47 mg, 18% yield). ^{1}H NMR (C_6D_6, 300 MHz): δ 20.1, 16.7, 11.3, 9.5, 8.7, 7.9, 7.7, -1.4, -5.0, -83.7. UV-vis (C_6H_6) λ_{max}, nm (ε): 578 (550), 778 (270). Evans Method (C_6D_6, 298 K): 3.75 μ_B. Electrochemistry (vs. ferrocene in THF with [TBA][PF_6] as supporting electrolyte): Co^{II}/Co^{III}, -300 mV; Co^{I}/Co^{II}, -1310 mV. Anal. Calcd for $C_{64}H_{56}BCoOP_3$: C, 76.58; H, 5.62. Found: C, 76.23; H, 5.88.

Additional ^{1}H NMR data for [PhBP$^{i\mathrm{Pr}}_3$]CoI, 4.12. ^{1}H NMR (C_6D_6, 300 MHz): δ 115.6 (6 H, T_1 = 2.6 ms, $PhB(CH_2P^iPr_2)_3$ or $P(CH(CH_3)_2)_2$), 41.6 (6 H, T_1 = 0.9 ms, $PhB(CH_2P^iPr_2)_3$ or $P(CH(CH_3)_2)_2$), 24.1 (18 H, T_1 = 5.6 ms, $P(CH(CH_3)_2)_2$), 12.8 (2 H, T_1

= 17.5 ms, *ortho* B(C_6H_5)), 9.0 (1 H, T_1 = 204 ms, *para* B(C_6H_5)), 7.3 (2 H, T_1 = 244 ms, *meta* B(C_6H_5)), 3.3 (18 H, T_1 = 1.9 ms, P(CH(CH_3)$_2$)$_2$).

Synthesis of [PhBP$^{iPr}_3$]CoOSiPh$_3$, 4.13. A THF solution (2 mL) of the thallium reagent TlOSiPh$_3$ (58 mg, 0.12 mmol) was added to a stirring THF solution (5 mL) of [PhBP$^{iPr}_3$]CoI, **4.12** (81 mg, 0.12 mmol). The solution was stirred for 1 h, and a yellow precipitate formed (TlI). The precipitate was removed by filtration over diatomaceous earth. The remaining reaction volatiles were removed in vacuo, and the purple powder was redisolved in benzene (5 mL). The benzene solution was filtered over diatomaceous earth to remove any residual TlI and then frozen and lyophilized to remove any trace of THF. Vapor diffusion of petroleum ether into a benzene solution (1 mL) afforded purple crystalline product (39 mg, 41% yield). ^{1}H NMR (C_6D_6, 300 MHz): δ 32.8, 21.6, 12.1, 11.0, 9.2, 8.9, 7.5, 7.4, 1.7, -60.3. UV-vis (C_6H_6) λ_{max}, nm (ε): 553 (600), 657 (380), 788 (320). Evans Method (C_6D_6): 4.32 μ_B. Electrochemistry (vs. ferrocene in THF with [TBA][PF_6] as supporting electrolyte): Co^{II}/Co^{III}, 100 mV (irreversible); Co^{I}/Co^{II}, -1690 mV. Anal. Calcd for $C_{45}H_{68}BCoOP_3Si$: C, 66.25; H, 8.40. Found: C, 66.20; H, 8.14.

Synthesis of [PhBP$^{iPr}_3$]CoSSiPh$_3$, 4.14. Followed protocol for **4.13**. Used TlSSiPh$_3$ (161 mg, 0.325 mmol) and **4.12** (216 mg, 0.325 mmol). Green crystals of **4.14** were isolated (167 mg, 62% yield). ^{1}H NMR (C_6D_6, 300 MHz): δ 35.7, 20.7, 11.4, 9.3, 8.7, 7.8, 7.1, 6.2, 5.0, -52.6. UV-vis (C_6H_6) λ_{max}, nm (ε): 604 (420), 664 (520), 747 (1300). Evans Method (C_6D_6): 4.00 μ_B. Electrochemistry (vs. ferrocene in THF with [TBA][PF_6] as supporting electrolyte): Co^{II}/Co^{III}, -140 mV (irreversible), Co^{I}/Co^{II}, -1330 mV. Anal. Calcd for $C_{45}H_{68}BCoP_3SSi$: C, 64.97; H, 8.24. Found: C, 64.77; H, 8.28.

Synthesis of {[PhBP$_3$]CoOSiPh$_3$}{BAr$_4$}, {4.15}{BAr$_4$}. Solid [PhBP$_3$]CoOSiPh$_3$, **4.1**, (98 mg, 0.096 mmol) and {[Cp]$_2$Fe}{B(3,5-(CF$_3$)$_2$-Ph)$_4$} (101 mg, 0.096 mmol) were added to a 20 mL vial and then THF (8 mL) was added. The solution immediately went from purple to green and was stirred for 10 min. The reaction mixture was then dried in vacuo to leave a green powder, which was washed with petroleum ether (3 x 10 mL). The green powder was dried to leave the pure product (140 mg, 77% yield), which was stored at –35 ºC. A similar procedure was used with {[Cp]$_2$Fe}{BPh$_4$} as the oxidant giving the less soluble counteranion (for X-ray crystallography). In this case the dried product was washed with a petroleum ether/benzene mixture (7:3) (3 x 10 mL) to give the final product (51% yield). A single crystal was grown at -35 °C in CH_2Cl_2 using the {BPh$_4$} counteranion. For {**4.15**}{B(3,5-(CF$_3$)$_2$-Ph)$_4$}: ^{1}H NMR (C_6D_6, 300 MHz): δ 8.43 (s, 8 H, *ortho* B(3,5-(CF$_3$)$_2$-C$_6$*H*$_3$)$_4$), 7.81 (d, J = 6.0 Hz, 8 H, *ortho* Si(C$_6$*H*$_5$)$_3$ and *ortho* B(C$_6$*H*$_5$)), 7.67 (t, J = 7.5 Hz, 2 H, *meta* B(C$_6$*H*$_5$)), 7.60 (s, 4 H, *para* B(3,5-(CF$_3$)$_2$-C$_6$*H*$_3$)$_4$), 7.47 (t, J = 7.5 Hz, 1 H, *para* B(C$_6$*H*$_5$)), 7.28 (m, 9 H, *meta* and *para* Si(C$_6$*H*$_5$)$_3$), 7.10 (m, 12 H, *ortho* P(C$_6$*H*$_5$)$_2$), 6.67 (t, J = 7.2 Hz, 6 H, *para* P(C$_6$*H*$_5$)$_2$), 6.40 (t, J = 7.5 Hz, 12 H, *meta* P(C$_6$*H*$_5$)$_2$), 0.98 (br s, 6 H, PhB(C*H*$_2$PPh$_2$)$_3$). ^{31}P{^{1}H} NMR (C_6D_6, 121.4 MHz): δ 64.6. ^{19}F{^{1}H} NMR (C_6D_6, 282 MHz): -58.5. UV-vis (C_6D_6) λ_{max}, nm (ε): 624 (830). Anal. Calcd for $C_{95}H_{68}B_2CoF_{24}OP_3Si$: C, 60.59; H, 3.64. Found: C, 60.59; H, 4.00. For {**4.15**}{BPh$_4$}: Identical UV-vis and ^{31}P NMR were found for the substituted anion.

Synthesis of [Tp$^{3,5\text{-}Me2}$]CoS(2,6-Me$_2$-Ph), 4.16. Anhydrous $CoBr_2$ (61.8 mg, 0.285 mmol) was slurried in THF (13 mL) for 10 min. Solid [K][Tp$^{3,5\text{-}Me2}$] (0.113 g, 0.335 mmol) was added over 30 min. To this solution, TlS(2,6-Me$_2$-Ph) (0.114 g, 0.335 mmol)

was added as a THF (3 mL) slurry and stirred for 30 min. After the addition of the thallium reagent, the solution turned green and white precipitate appeared (TlBr). The solution was filtered over Celite and then dried in vacuo to leave a green powder. The green powder was taken up in toluene (3 mL) and then crystallized by vapor diffusion of petroleum ether giving green crystals (0.043 g, 31% yield). Additional crystallizations can be used to collect additional product giving 69% total yield. ^{1}H NMR (C_6D_6, 300 MHz): δ 68.1, 38.5, 29.4, 16.2, -0.8, -11.4, -38.8. UV-vis (C_6H_6) λ_{max}, nm (ε): 647 (1300). SQUID (10-300 K): χT_{av} = 2.41 cm^3 K mol^{-1}. Anal. Calcd for $C_{23}H_{31}BCoN_6S$: C, 55.99; H, 6.33; N, 17.03. Found: C, 55.72; H, 6.23; N, 17.12.

4.4.6 X-ray experimental information

The general X-ray experimental procedure was performed according to section 2.4.4. Crystallographic information is provided in Table 4.6.

Table 4.6. X-ray diffraction experimental details for $[PhBP_3]CoOSiPh_3$ (**4.1**), $[PhBP_3]CoO(4\text{-}^tBu\text{-}Ph)$ (**4.2**), $[PhBP_3]CoSPh$ (**4.4**), $[PhBP_3]CoS(2,6\text{-}Me_2\text{-}Ph)$ (**4.5**), $[PhBP_3]CoS(2,4,6\text{-}^iPr_3\text{-}Ph)$ (**4.6**), $[PhBP_3]CoS(2,4,6\text{-}^tBu_3\text{-}Ph)$ (**4.7**), $[PhBP_3]CoSSiPh_3$ (**4.8**), $[PhBP_3]CoOSi(4\text{-}NMe_2\text{-}Ph)_3$ (**4.9**), $[PhBP_3]CoOCPh_3$ (**4.11**), $[PhBP^{iPr}_3]CoSSiPh_3$ (**4.14**), $\{[PhBP_3]CoOSiPh_3\}\{BPh_4\}$, $\{$**4.15**$\}\{BPh_4\}$, and $[Tp^{3,5\text{-}Me2}]CoS(2,6\text{-}Me_2\text{-}Ph)$, (**4.16**).

	$[PhBP_3]CoOSiPh_3$, (**4.1**)	$[PhBP_3]CoO(4\text{-}^tBu\text{-}Ph)$, (**4.2**)
Chemical formula	$C_{63}H_{56}BOP_3SiCo \cdot 1½(C_6H_6)$	$C_{55}H_{54}BCoOP_3$
Formula weight	1136.98	893.63
T (K)	98	98
λ (Å)	0.71073	0.71073
a (Å)	13.1013(14)	38.2238(8)
b (Å)	14.4428(16)	38.2238(8)
c (Å)	16.9894(19)	12.4091(5)
α (º)	77.984(2)	90
β (º)	67.962(1)	90
γ (º)	89.536(2)	90
V ($Å^3$)	2905.8(6)	18130.4(9)
Space group	$P\bar{1}$	$I4_1/a$
Z	2	16
Dcalcd (g/cm^3)	1.299	1.310
μ(cm^{-1})	4.44	5.25
R1, wR2 ($I>2\sigma(I)$)[a]	0.0336, 0.0673	0.0560, 0.0808

[a] $R1 = \Sigma \, | \, |F_o| - |F_c| \, | \, / \, \Sigma \, |F_o|$, $wR2 = \{ \, \Sigma \, [\, w(F_o^2 - F_c^2)^2 \,] \, / \, \Sigma \, [\, w(F_o^2)^2 \,] \, \}^{1/2}$

Table 4.6 (cont.)

	$[PhBP_3]CoSPh$, (**4.4**)	$[PhBP_3]CoS(2,6\text{-}Me_2\text{-}Ph)$, (**4.5**)
Chemical formula	$C_{51}H_{41}BCoP_3S$	$C_{53}H_{50}BCoP_3S$
Formula weight	853.59	881.64
T (K)	98	98
λ (Å)	0.71073	0.71073
a (Å)	16.8066(16)	12.0158(9)
b (Å)	14.0767(13)	12.5469(9)
c (Å)	19.2736(18)	15.5078(12)
α (º)	90	77.780(1)
β (º)	113.801(2)	77.546(1)
γ (º)	90	77.919(1)
V ($Å^3$)	4172.0(7)	2198.2(3)
Space group	$P2_1$	$P\bar{1}$
Z	4	2
Dcalcd (g/cm^3)	1.359	1.332
μ(cm^{-1})	6.10	5.80
R1, wR2 ($I>2\sigma(I)$)[a]	0.0463, 0.0661	0.0405, 0.0743

Table 4.6 (cont.)

	[PhBP$_3$]CoS(2,4,6-^{i}Pr$_3$-Ph), (**4.6**)	[PhBP$_3$]CoS(2,4,6-^{t}Bu$_3$-Ph), (**4.7**)
Chemical formula	$C_{60}H_{64}BCoP_3S$	$C_{63}H_{70}BCoP_3S \cdot C_6H_6$
Formula weight	979.82	1100.01
T (K)	98	98
λ (Å)	0.71073	0.71073
a (Å)	15.3738(11)	13.8333(10)
b (Å)	17.3171(13)	13.9539(10)
c (Å)	20.7953(15)	17.5922(13)
α (º)	65.655(1)	99.145(1)
β (º)	87.329(2)	106.587(1)
γ (º)	88.642(2)	107.029(1)
V (Å^3)	5038.5(6)	3000.8(4)
Space group	P$\bar{1}$	P$\bar{1}$
Z	4	2
Dcalcd (g/cm^3)	1.292	1.217
μ(cm^{-1})	5.20	4.40
R1, wR2 (I>2σ(I))[a]	0.0482, 0.0836	0.0663, 0.1133

Table 4.6 (cont.)

	$[PhBP_3]CoSSiPh_3$, (**4.8**)	$[PhBP_3]CoOSi(4\text{-}NMe_2\text{-}Ph)_3$, (**4.9**)
Chemical formula	$C_{63}H_{56}BCoP_3SSi \cdot 2\ C_6H_6$	$C_{69}H_{71}BCoN_3OP_3Si$
Formula weight	1192.09	1149.03
T (K)	98	98
λ (Å)	0.71073	0.71073
a (Å)	11.0416(8)	12.1092(11)
b (Å)	12.8426(9)	12.3919(11)
c (Å)	22.3975(15)	21.3227(19)
α (º)	87.228(1)	80.696(2)
β (º)	81.435(1)	75.993(2)
γ (º)	73.024(1)	72.962(1)
V ($Å^3$)	3003.7(4)	2954.0(5)
Space group	$P\bar{1}$	$P\bar{1}$
Z	2	2
Dcalcd (g/cm^3)	1.318	1.292
μ(cm^{-1})	4.70	4.40
R1, wR2 ($I>2\sigma(I)$)[a]	0.0529, 0.0777	0.0485, 0.0712

Table 4.6 (cont.)

	$[PhBP_3]CoOCPh_3$, (**4.11**)	$[PhBP^{iPr}_3]CoSSiPh_3$, (**4.14**)
Chemical formula	$C_{64}H_{56}BCoOP_3 \cdot C_6H_6$	$C_{45}H_{68}BCoP_3SSi$
Formula weight	1081.85	831.79
T (K)	98	98
λ (Å)	0.71073	0.71073
a (Å)	12.9420(10)	10.3161(4)
b (Å)	20.8485(15)	14.4678(6)
c (Å)	21.5457(16)	29.963(1)
α (º)	77.529(1)	90
β (º)	82.143(1)	90
γ (º)	88.626(1)	90
V ($Å^3$)	5622.9(7)	4472.0(3)
Space group	$P\bar{1}$	$P2_12_12_1$
Z	4	4
Dcalcd (g/cm^3)	1.278	1.235
μ(cm^{-1})	4.40	6.00
R1, wR2 ($I>2\sigma(I)$)[a]	0.0457, 0.0867	0.0431, 0.0606

Table 4.6 (cont.)

	{[PhBP$_3$]CoOSiPh$_3$}{BPh$_4$}, ({**4.15**}{BPh$_4$})	[Tp$^{3,5\text{-}Me2}$]CoS(2,6-Me$_2$-Ph), (**4.16**)
Chemical formula	$C_{87}H_{76}B_2CoOP_3Si \cdot 1½\ CH_2Cl_2$	$C_{23}H_{31}BCoN_6S$
Formula weight	1466.50	493.34
T (K)	98	98
λ (Å)	0.71073	0.71073
a (Å)	13.592(2)	23.0774(18)
b (Å)	14.814(2)	13.6982(10)
c (Å)	19.251(3)	7.9439(6)
α (º)	72.567(3)	90
β (º)	87.945(3)	90
γ (º)	82.565(2)	90
V (Å^3)	3667.0(9)	2511.2(3)
Space group	$P\bar{1}$	P_{nma}
Z	2	4
Dcalcd (g/cm^3)	1.328	1.305
μ(cm^{-1})	4.70	7.90
R1, wR2 (I>2σ(I))[a]	0.0643, 0.1156	0.0468, 0.0722

References cited

1) a) Nishida, Y.; Kida, S. *Bull. Chem. Soc. Jpn.* **1978**, *51*, 143-149. b) Gray, H. B. *Chemical Bonds: An Introduction to Atomic and Molecular Structure*; University Science Books: Mill Valley, CA, 1994.

2) a) Strauss, S. H.; Silver, M. E.; Long, K. M.; Thomson, R. G.; Hudgens, R. A.; Spartalian, K.; Ibers, J. A. *J. Am. Chem. Soc.* **1985**, *107*, 4207-4215. b) Goedken, V. L.; Pluth, J. J.; Peng, S.; Bursten, B. *J. Am. Chem. Soc.* **1976**, *98*, 8014-8021.

3) a) Solomon, E. I.; Rawlings, J.; McMillin, J. R.; Stephens, P. J.; Gray, H. B. *J. Am. Chem. Soc.* **1976**, *98*, 8046-8048. b) Bertini, I.; Luchinat, C. *Acc. Chem. Res.* **1983**, *16*, 272-279. c) Bertini, I.; Lanini, G.; Luchinat, C. *J. Am. Chem. Soc.* **1983**, *105*, 5116-5118. d) Khalifah, R. G.; Rogers, J. I.; Harmon, P. J.; Carroll, S. B. *Biochemistry* **1984**, *23*, 3129-3136. e) Briganti, F.; Pierattelli, R.; Scozzafava, A.; Supuran, C. T. *Eur. J. Med. Chem.* **1996**, *31*, 1001-1010.

4) Maret, W.; Vallee, B. L. "*Cobalt as probe and label of proteins*," *Methods in Enzymology* **1993**, *226*, 52-71.

5) a) Lippard, S. J.; Berg, J. M. *Principles of Bioinorganic Chemistry*; University Science Books: Mill Valley, CA, 1994; Chapter 12. b) Bren, K. L.; Pecoraro, V. L.; Gray, H. B. *Inorg. Chem.* **2004**, *43*, 7894-7896.

6) a) Lever, A. B. P. *Inorganic Electronic Spectroscopy*, 2nd ed.; Elsevier: New York, 1984; pp 480-505. b) Cotton, F. A.; Wilkinson, G. *Advanced Inorganic Chemistry*, 5th ed.; Wiley: New York, 1988; p. 729.

7) For examples of low spin Co(II) octahedral systems see: a) Faus, J.; Julve, M.; Lloret, F.; Muñoz, M. C. *Inorg. Chem.* **1993**, *32*, 2013-2017. b) Santra, B. K.; Lahiri, G. K. *J. Chem. Soc.*, *Dalton Trans.* **1998**, 139-145. c) Iwatsuki, S.; Obeyama, K.; Koshino, N.; Funahashi, S.; Kashiwabara, K.; Suzuki, T.; Takagi, H. D. *Can. J. Chem.* **2001**, *79*, 1344-1351. d) Reinen, D.; Ozarowski, A.; Jakob, B.; Pebler, J.; Stratemeier, H.; Wieghardt, K.; Tolksdorf, I. *Inorg. Chem.* **1987**, *26*, 4010-4017.

8) a) Zarembowitch, J. *New J. Chem.* **1992**, *16*, 255-267. b) Juhász, G.; Hayami, S.; Inoue, K.; Maeda, Y. *Chem. Lett.* **2003**, *32*, 882-883. c) Sieber, R.; Decurtins, S.; Stoeckli-Evans, H.; Wilson, C.; Yufit, D.; Howard, J. A. K.; Capelli, S. C.; Hauser, A. *Chem. Eur. J.* **2000**, *6*, 361-368. d) Gaspar, A. B.; Muñoz, M. C.; Niel, V.; Real, J. A. *Inorg. Chem.* **2001**, *40*, 9-10. e) Faus, J.; Julve, M.; Lloret, F.; Real, J. A.; Sletten, J. *Inorg. Chem.* **1994**, *33*, 5535-5540. f) Kremer, S.; Henke, W.; Reinen, D. *Inorg. Chem.* **1982**, *21*, 3013-3022.

9) For $[Cp]_2Co$ see: a) Gordon, K. R.; Warren, K. D. *Inorg. Chem.* **1978**, *17*, 987-994. b) König, E.; Schnakig, R.; Kremer, S.; Kanellakopulos, B.; Klenze, R. *Chem. Phys.* **1978**, *27*, 331-344. c) Warren, K. D. *Struct. and Bond.* **1976**, *27*, 45-159. For mixed-sandwich complexes see: d) Brunker, T. J.; Barlow, S.; O'Hare, D. *Chem. Commun*. **2001**, 2052-2053. e) Brunker, T. J.; Crowley, A. R.; O'Hare, D. *Organometallics* **2002**, *21*, 3123-3138. f) Brunker, T. J.; Green, J. C.; O'Hare, D. *Inorg. Chem.* **2003**, *42*, 4366-4381.

10) a) Sacconi, L. *Coord. Chem. Rev.* **1972**, *8*, 351-367. b) Morassi, R.; Bertini, I.; Sacconi, L. *Coord. Chem. Rev.* **1973**, *11*, 343-402.

11) a) Kennedy, B. J.; Murray, K. S. *Inorg. Chim. Acta* **1987**, *134*, 249-254. b) Kennedy, B. J.; Fallon, G. D.; Gatehouse, B. M. K. C.; Murray, K. S. *Inorg. Chem.* **1984**, *23*, 580-588.

12) a) Thuéry, P.; Zarembowitch, J. *Inorg. Chem.* **1986**, *25*, 2001-2008. b) Zarembowitch, J.; Kahn, O. *Inorg. Chem.* **1984**, *23*, 589-593.

13) Cirera, J.; Alemany, P.; Alvarez, S. *Chem. Eur. J.* **2004**, *10*, 190-207.

14) See Chapter 2 and Shapiro, I. R.; Jenkins, D. M.; Thomas, J. C.; Day, M. W.; Peters, J. C. *Chem. Commun.* **2001**, 2152-2153.

15) See Chapter 3 and Jenkins, D. M.; Di Bilio, A. J.; Allen, M. J.; Betley, T. A.; Peters, J. C. *J. Am. Chem. Soc.* **2002**, *124*, 15336-15350.

16) Jenkins, D. M.; Peters, J. C. *J. Am. Chem. Soc.* **2003**, *125*, 11162-11163.

17) a) Ray, M.; Hammes, B. S.; Yap, G. P. A.; Rheingold, A. L.; Borovik, A. S. *Inorg. Chem.* **1998**, *37*, 1527-1532. b) Sacconi, L.; Orlandini, A.; Midollini, S. *Inorg. Chem.* **1974**, *13*, 2850-2859. c) Mani, F.; Mealli, C. *Inorg. Chim. Acta* **1981**, *54*, L77-L79.

18) Holm, R. H. *Acc. Chem. Res.* **1969**, *2*, 307-316.

19) Jaynes, B. S.; Doerrer, L. H.; Liu, S.; Lippard, S. J. *Inorg. Chem.* **1995**, *34*, 5735-5744.

20) a) Everett, G. W.; Holm, R. H. *J. Am. Chem. Soc.* **1965**, *87*, 5266-6267. b) Cotton, F. A.; Soderberg, R. H. *J. Am. Chem. Soc.* **1962**, *84*, 872-873.

21) The complex {[$PhBP_3$]Fe≡N(1-Ad)}{NBu_4} has been thoroughly characterized (including by XRD analysis) and features a singlet ground state. Brown, S. D.; Peters, J. C. *J. Am. Chem. Soc.* (*accepted*).

22) Brown, S. D.; Betley, T. A.; Peters, J. C. *J. Am. Chem. Soc.* **2003**, *125*, 322-323.

23) Betley, T. A.; Peters, J. C. *J. Am. Chem. Soc.* **2003**, *125*, 10782-10783.

24) Betley, T. A.; Peters, J. C. *J. Am. Chem. Soc.* **2004**, *126*, 6252-6254.

25) Betley, T. A.; Peters, J. C. *Inorg. Chem.* **2003**, *43*, 5074-5084.

26) Brown, S. D.; Peters, J. C. *J. Am. Chem. Soc.* **2004**, *126*, 4538-4539.

27) Daida, E. J.; Peters, J. C. *Inorg. Chem*. **2004**, *43*, 7474-7485.

28) a) Reinaud, O. M.; Rheingold, A. L.; Theopold, K. H. *Inorg. Chem.* **1994**, *33*, 2306-2308. b) Detrich, J. L.; Konečný, R.; Vetter, W. M.; Doren, D.; Rheingold, A. L.; Theopold, K. H. *J. Am. Chem. Soc.* **1996**, *118*, 1703-1712. c) Jewson, J. D.; Liable-Sands, L. M.; Yap, G. P. A.; Rheingold, A. L.; Theopold, K. H. *Organometallics* **1999**, *18*, 300-305.

29) a) Shirasawa, N.; Akita, M.; Hikichi, S.; Moro-oka, Y. *Chem. Commun.* **1999**, 417-418. b) Shirasawa, N.; Nguyet, T. T.; Hikichi, S.; Moro-oka, Y.; Akita, M. *Organometallics* **2001**, *20*, 3582-3598.

30) a) Schebler, P. J.; Riordan, C. G.; Guzei, I. A.; Rheingold, A. L. *Inorg. Chem.* **1998**, *37*, 4754-4755. b) Schebler, P. J.; Mandimutsira, B. S.; Riordan, C. G.; Laible-Sands, L. M.; Incarvito, C. D.; Rheingold, A. L. *J. Am. Chem. Soc.* **2001**, *123*, 331-332.

31) a) Constable, E. C.; Baum, G.; Bill, E.; Dyson, R.; van Eldik, R.; Fenske, D.; Kaderli, S.; Morris, D.; Neubrand, A.; Neuburger, M.; Smith, D. R.; Wieghardt, K.; Zehnder, M.; Zuberbühler, A. D. *Chem. Eur. J.* **1999**, *5*, 498-508. And references therein. b) Sohrin, Y.; Kokusen, H.; Matsui, M. *Inorg. Chem.* **1995**, *34*, 3928-3934.

32) a) Bally, T.; Borden, W. T. *Rev. Comp. Chem.* **1999**, *13*, 1-97. b) Boone, A. J.; Chang, C. H.; Greene, S. N.; Herz, T.; Richards, N. G. J. *Coord. Chem. Rev.* **2003**, *238-239*, 291-314. c) Carreón-Macedo, J.; Harvey, J. N. *J. Am. Chem. Soc.* **2004**, *126*, 5789-5797.

33) a) Thompson, J. S.; Sorrell, T.; Marks, T. J.; Ibers, J. A. *J. Am. Chem. Soc.* **1979**, *101*, 4193-4201. b) Yoshimitsu, S.; Hikichi, S.; Akita, M. *Organometallics* **2002**, *21*, 3762-3773.

34) a) Jesson, J. P.; Trofimenko, S.; Eaton, D. R. *J. Am. Chem. Soc.* **1967**, *89*, 3148-3158. b) De Alwis, D.; Chanaka, L.; Schultz, F. A. *Inorg. Chem.* **2003**, *42*, 3616-3622.

35) a) Katzin, L. I. *J. Am. Chem. Soc.* **1954**, *76*, 3089-3090. b) Katzin, L. I.; Gebert, E. *J. Am. Chem. Soc.* **1953**, *75*, 2830-3832. c) Schmidtke, H.; Nover, J. *Inorg. Chem. Acta* **1995**, *240*, 231-237.

36) Hayashi, Y.; Yamamoto, T.; Yamamoto, A.; Komiya, S.; Kushi, Y. *J. Am. Chem. Soc.* **1986**, *108*, 385-391.

37) a) Kownacki, I.; Kubicki, M.; Marciniec, B. *Polyhedron* **2001**, *20*, 3015-3018. b) Osakada, K.; Takizawa, T.; Tanaka, M.; Yamamoto, T. *J. Organomet. Chem.* **1994**, *473*, 359-369. c) Tran, D. T. T.; Taylor, N. J.; Corrigan, J. F. *Angew. Chem., Int. Ed. Engl.* **2000**, *39*, 935-937.

38) Archibald, S. J.; Foxon, S. P.; Freeman, J. D.; Hobson, J. E.; Pernutz, R. N.; Walton, P. H. *J. Chem. Soc., Dalton Trans.* **2002**, 2797-2799.

39) The preparation was modified from this reference. See Experimental Section. Jazdzewski, B. A.; Holland, P. L.; Pink, M.; Young Jr., V. G.; Spencer, D. J. E.; Tolman, W. B. *Inorg. Chem.* **2001**, *40*, 6097-6107.

40) Ming, L. *Physical Methods in Bioinorganic Chemistry* (Ed.: L. Que, Jr.); University Science Books: Sausalito, CA, 2000, pp. 375-464.

41) MacBeth, C. E.; Thomas, J. C.; Betley, T. A.; Peters, J. C. *Inorg. Chem.* **2004**, *43*, 4645-4662.

42) Jenkins, D. M.; Betley, T. A.; Peters, J. C. *J. Am. Chem. Soc.*, **2002**, *124*, 11238-11239.

43) a) Avnir, D.; Katzenelson, O.; Keinan, S.; Pinsky, M.; Pinto, Y.; Salomon, Y.; Zabrodsky, H. *Concepts in Chemistry*: *A Contemporary Challenge* (Ed.: D. H. Rouvray); Research Studies Press: Taunton (UK), 1996. b) Alvarez, S.; Avnir, D.; Llunell, M.; Pinsky, M. *New J. Chem*. **2002**, *26*, 996-1009.

44) The atoms in the aryloxide ligand were refined isotropically.

45) For a discussion of EPR of Co(II) see: Banci, L.; Bencini, A.; Benelli, C.; Gatteschi, D.; Zanchini, C. *Struct. Bonding* **1982**, *52*, 37-86.

46) Stelzer, O.; Sheldrick, W. S.; Subramanian, J. *J. Chem. Soc., Dalton Trans.* **1976**, 966-970.

47) Palmer, G. *Physical Methods in Bioinorganic Chemistry* (Ed.: L. Que, Jr.); University Science Books: Sausalito, CA, 2000.

48) Gütlich, P.; Garcia, Y.; Goodwin, H. A. *Chem. Soc. Rev.* **2000**, *29*, 419-427.

49) We very recently obtained the solid-state crystal structure of the low spin half sandwich complex [$PhBP_3$]Co[Cp]. While a thorough discussion of this and related [BP_3]-supported half sandwich complexes is beyond the scope of this discussion, we note that in the crystalline state, [$PhBP_3$]Co[Cp] features a κ^3-bonding mode of the [$PhBP_3$] ligand and features one Co-P bond distance that is extremely distorted (2.479 Å) by comparison to the other two Co-P bond distances (2.242 Å and 2.231 Å). Jacobs, C. S.; Peters, J. C. *unpublished results*.

50) Sohn, Y. S.; Hendrickson, D. N.; Gray, H. B. *J. Am. Chem. Soc*. **1971**, *93*, 3603-3612.

51) Poli, R. *Chem. Rev*. **1996**, *96*, 2135-2204.

52) Jaguar 5.0, Schrodinger, LLC, Portland, Oregon, 2002.

53) Becke, A. D. *J. Chem. Phys.* **1993**, *98*, 5648-5652.

54) Lee, C.; Yang, W.; Parr R. G. *Phys. Rev. B* **1988**, *37*, 785-789.

55) SHAPE. Llunell, M.; Casanova, D.; Cirera, J.; Bofill, J. M.; Alemany, P.; Alvarez, S.; Pinsky, M.; Avnir, D. Version 1.1, Barcelona, 2003.

56) Harvey, S.; Lappert, M. F.; Raston, C. L.; Skelton, B. W.; Srivastava, G.; White, A. H. *J. Chem. Soc., Chem. Commun.* **1988**, *17*, 1216-1217.

57) Detty, M. R.; Wood, G. P. *J. Org. Chem.* **1980**, *45*, 80-89.

58) a) Oae, S.; Togo, H. *Bull. Chem. Soc. Jpn.* **1983**, *56*, 3802-3812. b) Blower, P. J.; Dilworth, J. R.; Hutchinson, J. P.; Zubieta, J. A. *J. Chem. Soc., Dalton Trans.* **1975**, 1533-1541.

59) Bochmann, M.; Webb, K. J. *Inorg. Synth.* **1997**, *31*, 158-162.

60) Gilman, H.; Plunkett, M. A.; Dunn, G. E. *J. Am. Chem. Soc.* **1951**, *73*, 1686-1688. Trichlorosiliane was substituted for tetrachlorosilane.

61) HOSi(*p*-CF_3-Ph) was prepared by the method of: Pauling, H.; Andrews, D. A.; Hindley, N. C. *Helv. Chim. Acta* **1976**, *59*, 1233-1243.

62) a) Connelly, N. G.; Geiger, W. E. *Chem. Rev.* **1996**, *96*, 877-910. b) Jordan, R. F.; LaPointe, R. E.; Bajgur, C. S.; Echols, S. F.; Willett, R. *J. Am. Chem. Soc.* **1987**, *109*, 4111-4113. c) Aggarwal, R. P.; Connelly, N. G.; Crespo, M. C.; Dunne, B. J.; Hopkins, P. M.; Orpen, A. G. *J. Chem. Soc., Dalton Trans.* **1992**, 655-662.

63) Le Bras, J.; Jiao, H.; Meyer, W. E.; Hampel, F.; Gladysz, J. A. *J. Organomet. Chem.* **2000**, *616*, 54-66.